Research Square

Preprints are preliminary reports that have not undergone peer review.
They should not be considered conclusive, used to inform clinical practice,
or referenced by the media as validated information.

Self-propulsion investigations for two AUV configurations using mesh topology optimization

Fei Deng

feideng880818@gmail.com

Xiamen Institute of Software Technology

Hongdong Yin

China University of petroleum (Beijing)

Article

Keywords: Mesh Topology Optimization, Open water, Straight-ahead, Self-propulsion, Velocity-pressure development, Verification and validation

Posted Date: November 12th, 2026

DOI: https://doi.org/10.21203/rs.3.rs-11480144/v1

License: This work is licensed under a Creative Commons Attribution 4.0 International License.
Read Full License

Additional Declarations:
No competing interests reported.

Declaration of interests

The authors declare that they have no known competing financial interests or personal relationships that could have appeared to influence the work reported in this paper.

The authors declare the following financial interests/personal relationships which may be considered as potential competing interests:

Self-propulsion investigations for two AUV configurations using mesh topology optimization

Fei Deng[a b*] Hongdong Yin[b]

([a] Full affiliation: Xiamen Institute of Software Technology, Xiamen, Fujian, China;
Detailed address: No. 1199, Sunban South Road, Jimei Education Zone, Xiamen, Fujian, China)

([b] Full affiliation: Department of earth physics, China University of petroleum (Beijing), Beijing, China;
Detailed address: NC.601, Road Fuxue.18, Changping, Beijing, China)

This manuscript is submitted to "Scientific Reports"

Running title: Self-propulsion investigation for AUV with mesh optimization

Index points:

1. The generic UV (Underwater vehicle) DARPA (Defense Advanced Research Projects Agency) Suboff and a typical propeller INSEAN (Italian National Institute for Naval Architecture Studies and Testing) E1619 will be numerically remodeled;
2. In pre-processing MTO (Mesh Topology Optimization) stage, 3D model geometry for Suboff and E1619, mathematical turbulence model, virtual computational flow domain resizing, meshing and near wall treatment, convergence study and uncertainty analysis for grid will be piecewise demonstrated;
3. Open water propeller analysis and straight-ahead resistance simulation will be conducted respectively in compliance with ITTC (International Towing Tank Conference) recommendations and guidelines to validate open water characters of E1619 propeller and underwater velocity-pressure development features of Suboff prototype on the basis of corresponding available EFD (Experimental Fluid Dynamics) data and previous empirical comparison CFD (Computational Fluid Dynamics) outcomes;
4. Self-propulsion simulation by means of body force method and full geometric model method will be correspondingly implemented on the foundation of aforementioned validation results to investigate vehicle self-propulsion points using thrust identity method and to assess hydrodynamic interaction effects between Suboff and E1619 via self-propulsion performance particulars;
5. By convention, relevant pre-processing MTO study outcomes and CFD simulation results will be presented and discussed in detail for further probable improvements.

Correspondence:
Name of corresponding author: Fei Deng
Email: feideng880818@gmail.com
Cellphone: 8618920520665
Fax: 8650184752240

Abstract

CFD (Computational Fluid Dynamics) topic raises great interest in recent years, especially involved with UVs (Underwater vehicles) and corresponding mounted propellers. In the sense of reality, before designing and manufacturing actual prototypes, pre-processing MTO (Mesh Topology Optimization) study and CFD simulation may be a secure, reliable, cost-effective and time-saving way to validate and investigate both detailed properties of prototype models and surrounding flow development according to previous empirical comparison CFD outcomes and accessible EFD (Experimental Fluid Dynamics) data. This paper develops open water propeller analysis, straight-ahead resistance simulation and self-propulsion simulation applied on the generic UV model namely DARPA (Defense Advanced Research Projects Agency) Suboff and a tailored propeller model called INSEAN (Italian National Institute for Naval Architecture Studies and Testing) E1619 using RANS (Reynolds averaging Navier-Stokes) two-equation Menter's k-ω SST (Shear Stress Transport) mathematical turbulence model with local mesh refinements, near wall treatment, convergence study and uncertainty analysis in pre-processing MTO stage of each case. MRF (Moving reference frame) method will be employed for open water propeller analysis to validate intrinsic open water characters of E1619 propeller. With regard to two bare form Suboff UV models (AFF-1 and AFF-8), vehicle total resistance along forward orientation, meridian distribution of dimensionless stress coefficient and average development distribution of wake stream-wise velocity profile will be respectively depicted and elaborated in straight-ahead resistance simulation. Furthermore, in the presence of E1619 propeller, self-propulsion interaction performance of Suboff UV seems to be sensitive to propeller open water characters and vehicle total resistance along forward orientation. Consequently, body force method and full geometric model method will be contrastively included into self-propulsion simulations for AFF-1 and AFF-8 Suboff models to investigate UV self-propulsion points using thrust identity method and to quantitatively assess corresponding hydrodynamic interaction effects between Suboff and E1619 by means of self-propulsion performance particulars, which is based on validation results in aforementioned open water and straight-ahead cases. By convention, pre-processing MTO study outcomes and CFD simulation results in regards to open water, straight-ahead and self-propulsion cases will be presented and discussed in detail.

Keywords:

Mesh Topology Optimization; Open water; Straight-ahead; Self-propulsion; Velocity-pressure development; Verification and validation

1. Introduction

In recent, CFD investigation trend is more than ever rapid, secure, increasingly reliable, standalone, cost-effective, conveniently versatile, compatible and time-saving. In this way, expanding its fields of applications and compatibility for both academic developments and practical industrial interest is imperative (Jiyuan Tu et al., 2013; Mojtaba Maali Amiri, 2018). In particular, a variety of open source and commercial simulation software are raised to further push up the application of CFD, like ANSYS, AQWA, COMSOL, Fluent, OpenFOAM, STAR CCM+, etc. Within computational unit such as hexahedral mesh grid, CFD simulation software is highly sensitive to capture the fluid dynamic details. Commercial CFD codes derived from FVM (Finite volume method) with high-fidelity solver are now widely utilized for plentiful underwater fluid dynamic issues, which is capable of simulating the flow around the UV hull or propeller not only under open water condition but also in non-uniform flow circumstance, even with perturbations from vehicle appendage

components (Philippe G. Ciarlet, 1978; Pijush K. Kundu and Ira M. Cohen, 2008). With higher mesh refinement costing and prolonging for computation cycle, CFD solver is possible to accurately capture wake distribution in specific extreme domains accompanied with highly transient effects (LeVeque and Randall J, 2006).

As to EFD (Experimental Fluid Dynamics), fluid hydrodynamic testing, prototype scale calibration, parameter adjustment and practical performance pre-assessment for UV or propeller in designing and testing stage will be important and indispensable issues for designers and researchers (Furkan KIYÇAK and Ömer Kemal KINACI, 2023). In fact, the complexity of the EFD work being done, the variability and the difficulty of environmental conditions is gaining with more uncertainty and instability (Yu Hsien Lin., 2018; Chunyu Guo et al., 2023). In this way, EFD research strategy might conversely be an undesirable option for practical interests in consideration of efficiency, security, realistic feasibility, repeatability, cost-effectiveness, versatility, compatibility and time-saving.

By contrast, CFD research strategy reinforced by modern FVM approach has already been benefit from fast development of the high-speed and sophisticate computer CPU (Central Processing Unit) technology rather than EFD. Albeit CFD simulations need to be validated in compliance with experiments and corresponding measurement data before further applications, CFD research strategy still shows a promising numerical processing performance in fluid dynamic analysis with aforementioned advantages (Kenshiro Takahashi, 2019).

With respect to propeller designing and assessing, open water propeller analysis is much fundamental. Tran Ngoc Tu (2019) presented simulation results of open water propeller analysis for a typical propeller model named PPTC based upon sixteen suites of initial and boundary conditions featuring mathematical turbulence model, grid type, computational flow domain scale and mesh refinement degree, which were able to reflect detailed influences from diverse initial and boundary conditions to final CFD simulation results. Eventually, author provided the most optimum initial and boundary condition with corresponding open water results for further investigation. Alexander B Phillips et al. (2008) specialized in the coupling of blade element momentum theory and RANS method for a generic propeller model mounted on UV stern. Uncertainty analysis had been executed to assess the grid type influence upon corresponding simulation process. In addition to rudder forces and moments, wake velocity profile distributions in stern propeller plane and mounted propeller particulars were emphatically investigated. In the research of Fabio Di Felice et al. (2009), numerical and model-scale experimental analyses for tailored prototype INSEAN E1619 propeller had been accomplished. Authors measured wake velocity profile distribution with the assistance of highly precise LDV (Laser Doppler Velocimetry) and simulated virtual computational flow domain in accordance with field test circumstance. In general, axial CFD simulation results deviate from physics assumptions and measurement data a bit with salient singularities and considerable error accumulations, probably on account of imprecise local mesh refinements.

In the past, hydrodynamic characteristics around a propeller surface could been studied in the presence of vehicle appendages relying on limited analytical or computational approaches (A. Nakayama and V. C. Patel F, 1973). Stern et al. (1994) adopted the crude viscous flow method for propeller model hydrodynamic investigations in the presence of vehicle hull. Computational viscous results had been compared with that acquired by means of flow potential theory and inviscid method, which seemed to indicate that viscous effects were too significant to be omitted. In this way, viscous flow method would gradually override conventional inviscid method in CFD research field. Jeong Hwa Seo et al. (2010) had conducted model-scale straight-ahead resistance simulation, open water propeller analysis and self-propulsion interaction performance simulation on the basis of KCS vehicle prototype and object KP505 propeller using RANS solver. Computational flow domain for open water propeller analysis in their work would be heuristically optimized by means of local sliding mesh refinements with grid uncertainty assessment. Corresponding relative errors between accessible experimental data and numerical results were fairly acceptable. In

addition, as another principal particulars, self-propulsion points should not be neglected in self-propulsion investigation. Carrica P. M et al. (2010) put forward a time consuming controller approach, namely, controlling propeller rotation speed to search self-propulsion points and to approximate target Froude number for the surface vehicle model, which was capable to shorten redundant CFD simulation cycles drastically via retaining merely one computational process. Corresponding numerical results in regard to KVLCC1, ONR Tumblehome and KCS integration models on the foundation of this approach could meet expectation in V&V (verification and validation). In the research of Yusuke Tahara et al. (2006), steady fluid dynamics had been analyzed using two different RANS solvers. Comparisons between available EFD data and CFD results for both towing tank and straight-ahead resistance tests were elaborated. Dmitriy Ponkratov and Constantinos Zegos (2015) employed MRF method and well-studied two-equation Menter's k-ω SST mathematical turbulence model in initial stage of CFD simulation process so as to compress the approximation period of numerical solutions. Full-scale self-propulsion simulation results showed satisfactory agreement with accessible field test data.

Moreover, benefit from rapid development of velocity-pressure discretization estimation techniques for non-uniform flow distribution in vehicle-propeller studies, so far, self-propulsion interaction effect investigation has received great attention from plenty of researchers (J.M.J. Journée and Jakob Pinkster, 2002; Mattias Liefvendahl et al., 2010; Yasemin Arıkan Ozden et al., 2017). Nathan Chase (2012) developed a comprehensive issue for open water characters, straight-ahead features and self-propulsion interaction performance in regards to well-known DARPA Suboff UV and seven bladed INSEAN E1619 propeller. An open source CFD solver called Ship-Iowa was adopted for open water propeller analysis under a consistent set of inlet flow initial conditions. Influences from different mathematical turbulence models and grid types to corresponding numerical consequences had been severally discussed in their study. Besides, the rudder-propeller distance and rake angle of rudder in stern region of UV prototype may have a dominant effect on self-propulsion interaction performance as well (Xuting Zhang et al., 2019). In this way, relevant rudder-propeller model system was established and investigated under different initial conditions with respect to rudder-propeller distances and rake angles of rudder. Optimum initial condition was proposed by authors to moderately mitigate pressure drop and vortices problems around rudder training edge and propeller blade guide curve.

Furthermore, for the sake of enhancing accuracy, applicability and robustness of self-propulsion interaction effect investigation, a variety of experimental and numerical approaches spring up. Based upon load-varying self-propulsion test method, Yasemin Arıkan Ozden et al. (2019) carried out a series of field tests meticulously for Suboff UV and E1619 propeller consisting of resistance tests and propulsion tests. Self-propulsion points, hull efficiency, relative rotation efficiency and propulsion efficiency EFD results measured under seven propeller rotation speed conditions were generally acceptable as expected. Yan Naing Win et al. (2013) had employed an optimized RANS solver coupled with quasi-steady blade element theory to investigate self-propulsion interaction effects between Series 60 vehicle hull and a five bladed fixed pitch propeller MAU, which considered straight-ahead and self-propulsion cases. In their work, generally low validation deviations between corresponding EFD and CFD results indicated that the remodeled propeller approach on the foundation of quasi-steady blade element theory was fairly promising. Cihad Delen et al. (2017) and Yung An Chu et al. (2018) applied body force method in propeller modeling stage of self-propulsion simulation empirically with corresponding numerical results, which demanded virtual actuator disk V&V instead of more conventional full-scale model test. Liwei Liu et al. (2021) conducted a quite systematic single phase CFD study for Suboff UV and E1619 propeller. Geometry modeling, mesh refinement, computational flow domain resizing, open water propeller analysis, straight-ahead investigation and self-propulsion prediction using thrust identity method had been included and fully discussed. In particular, uncertainty analysis in compliance with fine, medium and coarse grid types could contribute to highly credible, reasonable and applicable CFD

solutions in their paper.
Despite of more and more participants paying considerable efforts, the numerical research field in regard to self-propulsion UV is still cold-shouldered as before with a great deal of blank areas and black dots to be padded (Alexander V. Inzartsev, 2009; Nathan Chase and Pablo M. Carrica, 2013; Chunyu Guo et al., 2023). This paper primarily aims to investigate open water characters for E1619 propeller, straight-ahead features for Suboff UV and further self-propulsion interaction performance with assistance of corresponding pre-processing MTO studies highlighted in this work, which could be considered as a consistent datasheet for real prototype designing and apriori assessment.
In following chapters, after a short description with respect to geometry remodeling for both UV prototype DARPA Suboff and propeller prototype INSEAN E1619, mathematical turbulence model adopted in this paper will be introduced and explained. Moreover, a detailed MTO summary in regards to virtual computational flow domain resizing, meshing and near wall treatment in pre-processing stage will be elaborated, as well as convergence study and uncertainty analysis for grid (Patrick J. Roache, 1997; Tyrone S. Phillips and Christopher J. Roy, 2014). In addition, CFD OWCs (Open water curves), vehicle total resistances along forward orientation, meridian distributions of dimensionless stress coefficient, average development distributions of wake stream-wise velocity profile, UV self-propulsion points and self-propulsion performance particulars will be acquired step by step and discussed on the basis of accessible EFD validation data and previous empirical comparison CFD outcomes, which emphasize the flow velocity-pressure development investigation rather than conventional model identification.

2. Modeling

2.1 Geometry of Suboff UV

For academic interest purpose, generic DARPA Suboff model as a benchmark vehicle form is widely employed on account of abundant available experimental data and previous empirical research outcomes for further validations and comparisons (Han-Lieh Liu and Thomas T. Huang, 1998). As for this work, Suboff datasheets in regard to scale and configuration details are accessible in Nancy C. Groves et al. (1989) and Robert F. Roddy (1990). Meanwhile, vehicle remodeling procedures and considerations will strictly follow the ITTC (International Towing Tank Conference) recommendations and guidelines (ITTC, 2011b, 01. 7.5-03-02-03, 2011) for minor additive modeling error. In particular, two bare forms without propeller, namely, AFF-1 and AFF-8 will be individually investigated on the foundation of generic DARPA Suboff model. AFF-1 is the bare hull form while AFF-8 represents the fully appendage form including sail and stern fin geometric components (Thomas T. Huang et al., 1989). The general 3-D schematic view of AFF-1 and AFF-8 Suboff UV model with essential geometrical and physical particulars have been respectively presented in Fig. 1 and Table 1.

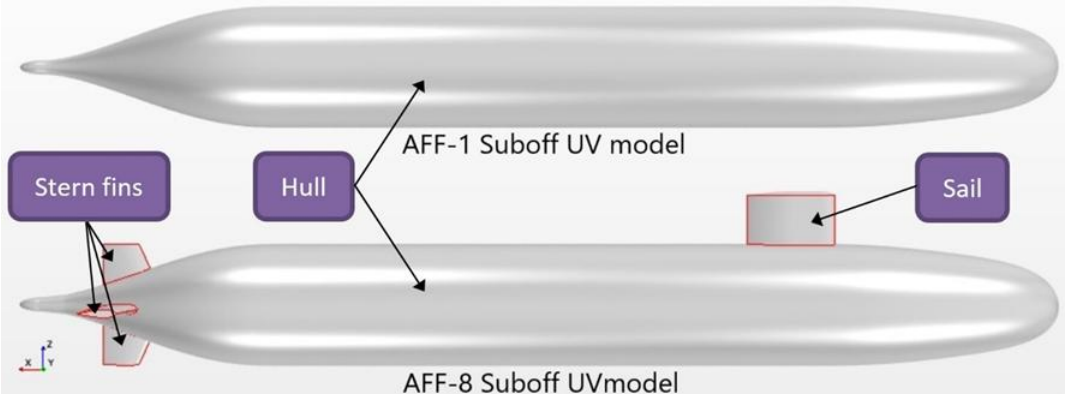


Fig. 1. General 3-D schematic view of AFF-1 and AFF-8 Suboff UV model

Table 1
Essential geometrical and physical particulars for two Suboff UV models.

Notation	Description	Unit	AFF-1	AFF-8
L_{OA}	Overall length	[m]	4.356	4.356
L_{CP}	Length between perpendiculars	[m]	4.261	4.261
D_{max}	Maximum hull diameter	[m]	0.508	0.508
S_{WA}	Wetted surface area	[m^2]	5.989	6.348
∇	Displacement volume	[m^3]	0.699	0.706
L_{CB}	Longitudinal center of buoyancy (Aft of nose)	[m]	$0.461L_{OA}$	$0.462L_{OA}$
λ	Linear scale ratio (Liwei Liu et al., 2021)	[-]	24	24

2.2 Geometry of E1619 propeller

E1619 propeller prototype was originally developed by INSEAN Propulsion and Cavitation Laboratory, which had been investigated in INSEAN basin for various field test purposes (Fabio Di Felice et al., 2009; Sinan Burunsuz et al., 2017). E1619 is a highly skewed seven-bladed propeller with the unloaded blade tip designing. In the light of tailored geometry of E1619 propeller, blade tip, blade guide curve, chord, rake angle, hub and nose cap will be finely tuned and calibrated on the basis of scale and configuration datasheets, relevant empirical CFD research outcomes and ITTC open water recommendations and guidelines (ITTC, 2014, 03. 7.5-02-03-02.1, 2014; Grabert R et al., 2017; Karim I et al., 2019; Ji Tao Qiu et al., 2022; Yu-Hsin Lin et al., 2023). Primary geometrical and physical particulars with respect to E1619 propeller model are annotated in Table 2. In addition, 3-D open water schematic view of INSEAN E1619 propeller model is depicted consisting of driven shaft, hub, propeller blade and nose cap geometric components, as Fig. 2.

Table 2

Primary geometrical and physical particulars with respect to E1619 propeller model.

Nomenclature	Description	Unit	Open water propeller case	Self-propulsion case
Z	Number of blades	[-]	7	7
D	Model-scale propeller diameter (Nathan Chase, 2012)	[m]	0.485	0.262
D_h/D	Hub diameter ratio	[-]	0.226	0.226
P/D	Propeller pitch ratio at 0.7R	[-]	1.15	1.15
R	Model-scale propeller radius	[m]	0.2425	0.131
$C_{0.75}$	Chord length of propeller blade at 0.75R	[m]	0.0068	0.0037
A_E/A_0	Expanded area ratio of propeller blade	[-]	0.608	0.608
L_{Shaft}	Length of driven shaft	[m]	7.1314	-

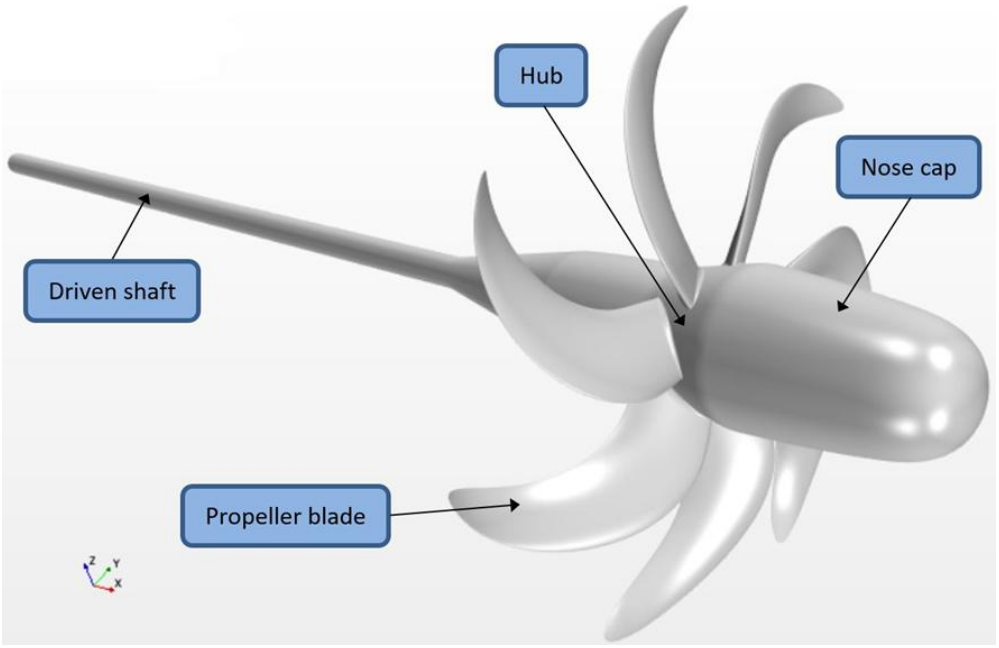


Fig. 2. 3-D open water schematic view of INSEAN E1619 propeller model

2.3 Mathematical turbulence model

In this paper, the continuity equation, foundational RANS momentum partial differential equation set and two-equation Menter's k-ω SST hybrid model will be included and elaborated for three dimensional flows. The generalized form of continuity equation is expressed as Eq. (1).

$$\frac{\partial \rho}{\partial t} + \nabla(\rho V) = 0 \tag{1}$$

Where, ρ denotes fluid density at 11 ℃ (ITTC, 2011, 02. 7.5-02-01-03, 2011). For the sake of restraining needless computational overhead, flow around model is hypothesized as incompressible. In this way, continuity equation is able to be simplified as Eqs. (2) and (3).

$$\frac{\partial \rho}{\partial t} = 0 \tag{2}$$

$$\nabla V = \frac{\partial u}{\partial x} + \frac{\partial v}{\partial y} + \frac{\partial w}{\partial z} = 0 \tag{3}$$

Where, u, v and w represent velocity components along three axial directions within global Cartesian O-NED (North east down) geographical inertial frame system (J.M.J. Journée and W.W. Massie, 2001), severally. With regard to incompressible flows ($\nabla V = 0$), the generalized N-S (Navier-Stokes) partial differential equation set can be expressed as Eq. (4).

$$\begin{cases} \frac{\partial u}{\partial t} + \frac{\partial u}{\partial x}\frac{\partial x}{\partial t} + \frac{\partial u}{\partial y}\frac{\partial y}{\partial t} + \frac{\partial u}{\partial z}\frac{\partial z}{\partial t} = -\frac{1}{\rho}\frac{\partial p}{\partial x} + \nu\nabla^2 u \\ \frac{\partial v}{\partial t} + \frac{\partial v}{\partial x}\frac{\partial x}{\partial t} + \frac{\partial v}{\partial y}\frac{\partial y}{\partial t} + \frac{\partial v}{\partial z}\frac{\partial z}{\partial t} = -\frac{1}{\rho}\frac{\partial p}{\partial y} + \nu\nabla^2 v \\ \frac{\partial w}{\partial t} + \frac{\partial w}{\partial x}\frac{\partial x}{\partial t} + \frac{\partial w}{\partial y}\frac{\partial y}{\partial t} + \frac{\partial w}{\partial z}\frac{\partial z}{\partial t} = -\frac{1}{\rho}\frac{\partial p}{\partial z} + \nu\nabla^2 w \end{cases} \tag{4}$$

Where, p denotes pressure. If generalized N-S equations are applied straightway to calculate the transient details of turbulent flows like DNS (Direct numerical simulation) strategy, a great deal of computational overhead will be consumed, which is unrealistic and unfeasible. In general, RA (Reynolds averaging) method needs to be adopted as a sort of INS (Indirect numerical simulation) strategy to estimate the mean velocity-pressure characteristics of turbulent flows via tuning the form of generalized N-S equations (David C.Wilcox, 2006; Gao Hongtao et al., 2019), which is called RANS momentum partial differential equation set, as Eq. (5).

$$\begin{cases} \rho\frac{\partial \bar{U}}{\partial t} + \rho\bar{U}\frac{\partial \bar{U}}{\partial x} + \rho\bar{V}\frac{\partial \bar{U}}{\partial y} + \rho\bar{W}\frac{\partial \bar{U}}{\partial z} = -\frac{\partial \bar{P}}{\partial x} + \mu\left[\frac{\partial^2 \bar{U}}{\partial^2 x} + \frac{\partial^2 \bar{U}}{\partial^2 y} + \frac{\partial^2 \bar{U}}{\partial^2 z}\right] - \rho\left[\frac{\partial \overline{u'^2}}{\partial x} + \frac{\partial \overline{v'u'}}{\partial y} + \frac{\partial \overline{w'u'}}{\partial z}\right] \\ \rho\frac{\partial \bar{V}}{\partial t} + \rho\bar{U}\frac{\partial \bar{V}}{\partial x} + \rho\bar{V}\frac{\partial \bar{V}}{\partial y} + \rho\bar{W}\frac{\partial \bar{V}}{\partial z} = -\frac{\partial \bar{P}}{\partial y} + \mu\left[\frac{\partial^2 \bar{V}}{\partial^2 x} + \frac{\partial^2 \bar{V}}{\partial^2 y} + \frac{\partial^2 \bar{V}}{\partial^2 z}\right] - \rho\left[\frac{\partial \overline{u'v'}}{\partial x} + \frac{\partial \overline{v'^2}}{\partial y} + \frac{\partial \overline{w'v'}}{\partial z}\right] \\ \rho\frac{\partial \bar{W}}{\partial t} + \rho\bar{U}\frac{\partial \bar{W}}{\partial x} + \rho\bar{V}\frac{\partial \bar{W}}{\partial y} + \rho\bar{W}\frac{\partial \bar{W}}{\partial z} = -\frac{\partial \bar{P}}{\partial z} + \mu\left[\frac{\partial^2 \bar{W}}{\partial^2 x} + \frac{\partial^2 \bar{W}}{\partial^2 y} + \frac{\partial^2 \bar{W}}{\partial^2 z}\right] - \rho\left[\frac{\partial \overline{u'w'}}{\partial x} + \frac{\partial \overline{v'w'}}{\partial y} + \frac{\partial \overline{w'^2}}{\partial z}\right] \end{cases} \tag{5}$$

In RANS momentum equations, $\overline{U}$, $\overline{V}$ and $\overline{W}$ represent three mean velocity components along each axial direction within global Cartesian O-NED geographical inertial frame system, respectively; u', v' and w' denote fluctuation velocity components along three axial directions, severally; $\overline{P}$ and μ represent mean pressure and dynamic viscosity, individually. In this work, two-equation Menter's k-ω SST hybrid mathematical turbulence model is employed to approximatively complete RANS momentum equations and to flexibly solve both turbulent boundary layer and far field fluid motion equations for UV and propeller models in a segregated manner. As a crux term, the Reynolds stress tensors $\overline{u_i'u_j'}$ are additionally derived during Reynolds averaging process from generalized N-S equations to RANS momentum equations (Jiyuan Tu et al., 2013), which can be assumed and constructed as following polynomial form:

$$\overline{u_i'u_j'} = \frac{\tau_{ij}}{-\rho} = -\nu_t\left(2S_{ij} - \frac{2}{3}\frac{\partial \overline{U_k}}{\partial x_k}\delta_{ij}\right) + \frac{2}{3}k\delta_{ij} \tag{6}$$

Where, ν_t represents the kinematic eddy-viscosity and will be hypothesized as $\nu_t = a_1 k/\max(a_1\omega, \Omega F_2)$; a_1 denotes an empirical closure constant; Ω is the absolute vorticity; F_2 represents a blending function as $F_2 = \tanh\left[\max^2\left(2\sqrt{k}/\beta^*\omega d, 500\nu/\omega d^2\right)\right]$ with the empirical closure constant β^*, the normal distance between abutting surface d and the laminar kinematic viscosity ν; S_{ij} denotes the average strain rate tensors, which can be expressed as: $S_{ij} = \left(\partial\overline{U_i}/\partial x_j + \partial\overline{U_j}/\partial x_i\right)/2$. In addition to $\overline{u_i'u_j'}$ and ν_t, two extra transport equations with auxiliary correlations (Florian R. Menter, 1993) need to be solved for undetermined turbulence kinetic energy k and specific turbulence dissipation rate ω, as Eqs. (7) to (14).

Extra transport equations:

$$\frac{\partial k}{\partial t} + \frac{\partial(k\overline{U_j})}{\partial x_j} = P_k - \beta^*\omega k + \frac{\partial}{\partial x_j}\left[(\nu + \sigma_k\nu_t)\frac{\partial k}{\partial x_j}\right] \tag{7}$$

$$\frac{\partial \omega}{\partial t} + \frac{\partial(\omega\overline{U_j})}{\partial x_j} = \frac{\gamma}{\nu_t}P_k - \beta\omega^2 + \frac{\partial}{\partial x_j}\left[(\nu + \sigma_\omega\nu_t)\frac{\partial \omega}{\partial x_j}\right] + 2(1-F_1)\frac{\sigma_{\omega 2}}{\omega}\frac{\partial k}{\partial x_j}\frac{\partial \omega}{\partial x_j} \tag{8}$$

Auxiliary correlations:

$$P_k = \frac{\tau_{ij}\partial\overline{U_i}}{\rho\,\partial x_j} \tag{9}$$

$$\tau_{ij} = \mu_t\left(2S_{ij} - \frac{2}{3}\frac{\partial\overline{U_k}}{\partial x_k}\delta_{ij}\right) - \frac{2}{3}\rho k\delta_{ij} \tag{10}$$

$$\mu_t = \rho\nu_t \tag{11}$$

$$\gamma = \frac{\beta}{\beta^*} - \frac{\sigma_\omega\kappa^2}{\sqrt{\beta^*}} \tag{12}$$

$$F_1 = \tanh\left\{\min^4\left[\max\left(\frac{\sqrt{k}}{\beta^*\omega d}, \frac{500\nu}{\omega d^2}\right), \frac{4\rho\sigma_{\omega 2}k}{CD_{k\omega}d^2}\right]\right\} \tag{13}$$

$$CD_{k\omega} = \max\left(2\rho\sigma_{\omega 2}\frac{\partial k}{\omega}\frac{\partial \omega}{\partial x_j}\frac{\partial \omega}{\partial x_j}, 10^{-20}\right) \tag{14}$$

Where, κ represents von Kármán constant, experimentally presupposed as 0.41 (B. Aupoix, 2014); σ_k, β and σ_ω denote hybrid closure constants, which will be finalized by means of following blending equation $\phi = F_1\phi_1 + (1-F_1)\phi_2$.

With restrained CFL (Courant-Frederich-Lewis) number to strengthen the numerical stability and robustness of aforementioned computational approaches.

According to Menter's SST turbulence theory (Florian R. Menter, 1994), subscript 1 arisen in blending functions and hybrid closure constants indicate k-ω turbulence model dominating while subscript 2 means k-ε dominating. In this way, non-uniform flows with adverse pressure gradient, strong curvature flows and separated flows around propeller blades, vehicle sail and stern fins in this work are able to be subtly estimated up to viscous sublayer of turbulent boundary layer on the basis of promising LRN (Low Reynolds number) k-ω turbulence model blended in Menter's SST hybrid methodology with limited robustness CFL (Courant-Frederich-Lewis) number and satisfying precision while HRN (High Reynolds number) k-ε turbulence model will solve free shear fluid motion equations in fully turbulent far field region with acceptable solution convergence rate, higher algorithm stability and minor computational overhead, which is equivalent to an advantage trade-off between k-ω and k-ε turbulence models.

2.4 Virtual computational flow domain

As illustrated in Fig. 3, virtual computational flow domain for E1619 open water propeller analysis primarily comprises four constituent regions: rotation region in regards to MRF method, static region, upstream region and downstream region, which will be preliminarily demarcated through conformal intersecting surfaces in accordance with the propeller mounted plane location.

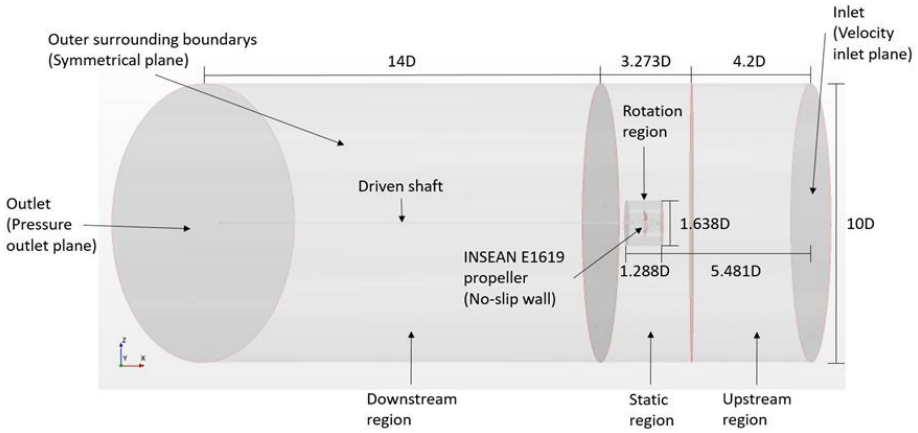


Fig. 3. Virtual computational flow domain for E1619 open water propeller analysis

In this work, boundary conditions of inlet, outlet and outer surrounding boundarys are severally preset as velocity inlet pane, pressure outlet plane and symmetrical plane while surfaces of propeller blade, hub, nose cap and driven shaft are defined as no-slip wall. E1619 propeller blades and hub are remodeled in rotation region and integrated with nose cap and driven shaft to simulate the realistic operating state of E1619 propeller in towing tank or circulating cavitation tunnel. In compliance with relevant empirical CFD research outcomes and ITTC open water recommendations and guidelines (ITTC, 2014, 03. 7.5-02-03-02.1, 2014; Mattias Liefvendahl, 2015; Ehsan Javanmard et al., 2019; Ji Tao Qiu et al., 2022; Yu-Hsin Lin et al., 2023), axial distance between velocity inlet plane and inlet plane of static region should not shorter than 2D to guarantee that velocity inlet plane is far away from E1619 propeller blades for minor inlet disturbances; Outer diameter of static region needs to be longer than 4D to sufficiently restrain boundary perturbations; Driven shaft length is supposed to be placed as 4D or longer for minor outlet disturbances.
In consideration of similar simulation circumstance, virtual computational flow domain scales corresponding to AFF-1 and AFF-8 Suboff models will be deemed as consistent in this paper, which is presented in Fig. 4. The right side and the left side of computational flow domain are respectively preset as velocity inlet plane and pressure outlet plane while vehicle surface is defined as no-slip wall; Outer surrounding boundarys are preset as symmetrical plane to demarcate a proper computational flow domain for UV simulations with minor outer boundary near wall effects (Furkan KIYÇAK and Ömer Kemal KINACI, 2023). In addition to boundary conditions, computational flow domain dimensions need to be moderately finalized as well on the basis of ITTC vehicle CFD recommendations and guidelines (ITTC, 2011b, 01. 7.5-03-02-03, 2011; ITTC, 2014, 00. 7.5-03-03-01, 2014) so that flow details around UV model in straight-ahead resistance simulation and self-propulsion simulation can be accurately captured without redundant computational overhead and implicit influences from flow domain dimensions to CFD results.

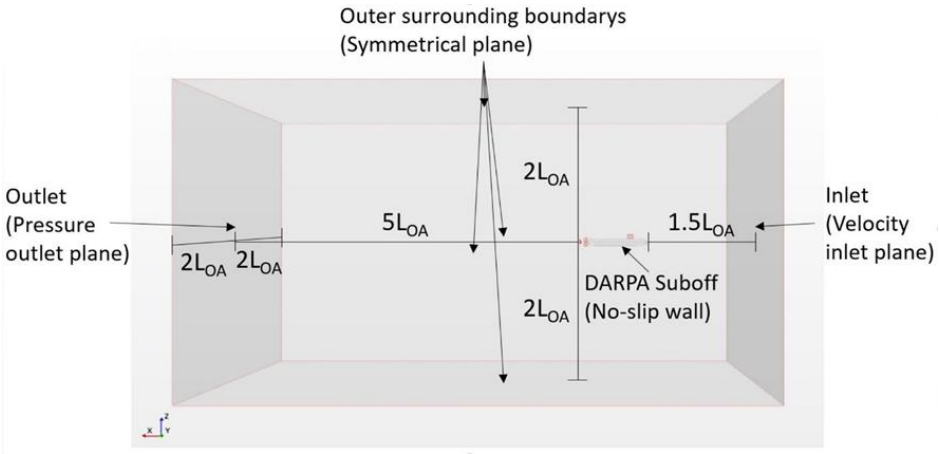


Fig. 4. Virtual computational flow domain for Suboff simulations

2.5 Mesh Topology Optimization

In this paper, virtual computational flow domain for each simulation case will be discretized by means of three dimensional finite grids in compliance with FVM to describe flow velocity-pressure development characteristics around UV or propeller model (John C. Strikwerda, 2004; Nathan Chase and Pablo M. Carrica, 2013), namely, the meshing.

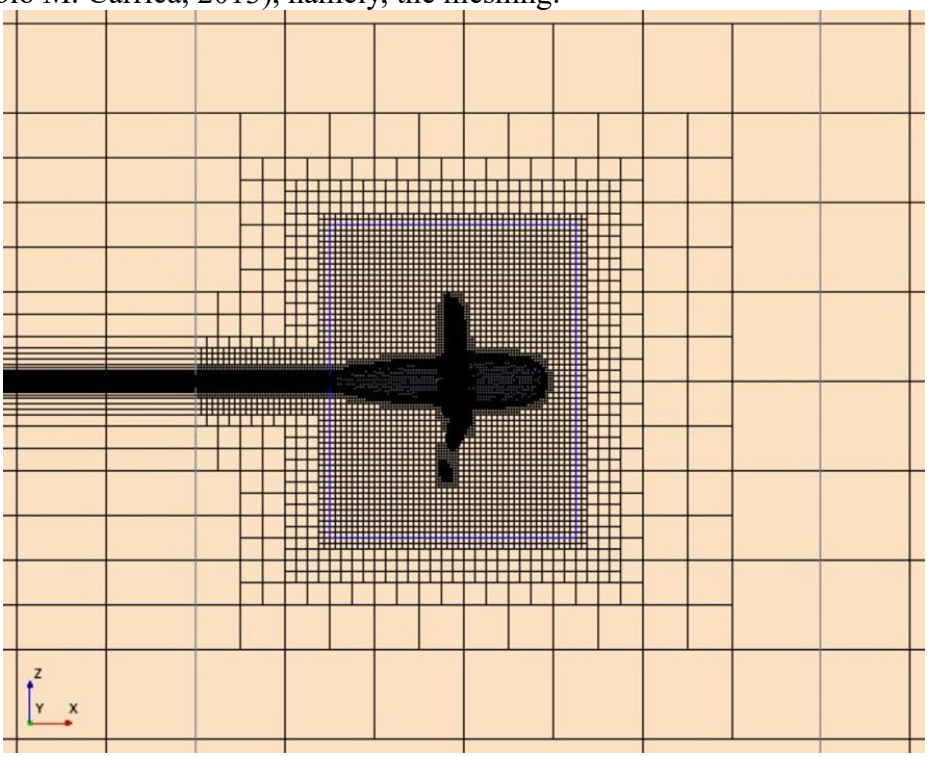


Fig. 5. Mesh layout for rotation region in E1619 open water propeller analysis

Fig. 5 depicts mesh layout for rotation region of virtual computational flow domain applied on open water propeller analysis, which will be enriched via extruder meshing method. Instead of tetrahedral cell, hexahedral trimmed cell algorithm is adopted for E1619 propeller model with surface mesher and prism layer mesher. With regard to most propeller advance coefficient cases, trimmer surface growth rate, prism layer total thickness and prism layer near wall thickness for propeller blades, hub, nose cap and driven shaft need to be tuned individually for the purpose of retaining desired wall y^+ values within an acceptable range around 1. Furthermore, local propeller mesh for blade guide curve and blade tip is refined as Fig. 6 to accurately capture more curvature flow details around propeller blades and to weaken stochastic computational instabilities or blade tip vortices

(D. Dussin et al., 2009; Ehsan Yari and Hassan Ghassemi, 2016).

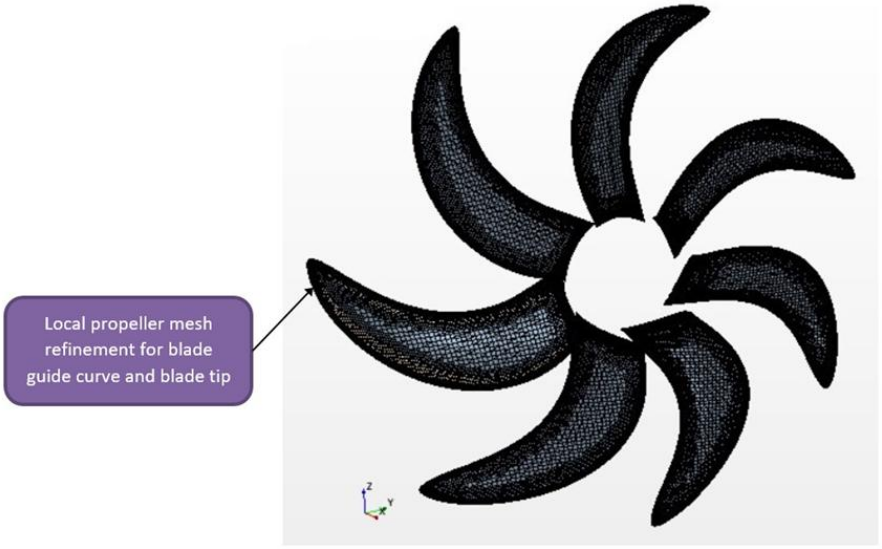


Fig. 6. Local propeller mesh refinement for blade guide curve and blade tip

As for AFF-1 and AFF-8 Suboff UV simulations, reasonable global mesh layouts will be foundationally established by means of hexahedral trimmed cell algorithm with second-order upwind convection scheme. Local surface meshes in nose, sail, sail wake, stern, stern fin, stern wake and self-propulsion rotation regions need to be refined for Suboff UV simulations, which could have a dominant effect on accuracy and applicability of final results. In addition, prism layer mesh is employed to subtly capture more near wall flow messages within model turbulent boundary layer and to mitigate pressure drop or CFD solution oscillatory convergence problem (Serge Toxopeus, 2008; Kenshiro Takahashi, 2019; Guanghua He et al., 2022). In this way, prism layer near wall thickness of first grid next to the model surface must be tuned precisely to maintain corresponding desired wall y^+ value within closed interval [1, 5] while most prism layer total thickness δ (Wall $y^+ = 1000$) will be adjusted to be not larger than surface mesh target size to ensure a smooth computational volume transition between last prism grid layer and core volumetric mesh (A. Drouet et al., 2011). Unstructured mesh layouts for both AFF-1 and AFF-8 Suboff UV model cases are presented in Figs. 7 and 8.

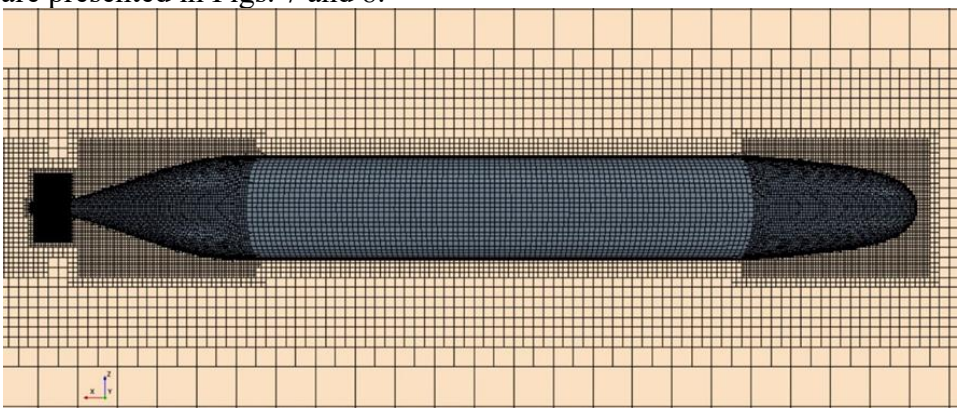


Fig. 7. Unstructured mesh layout for AFF-1 Suboff UV model cases

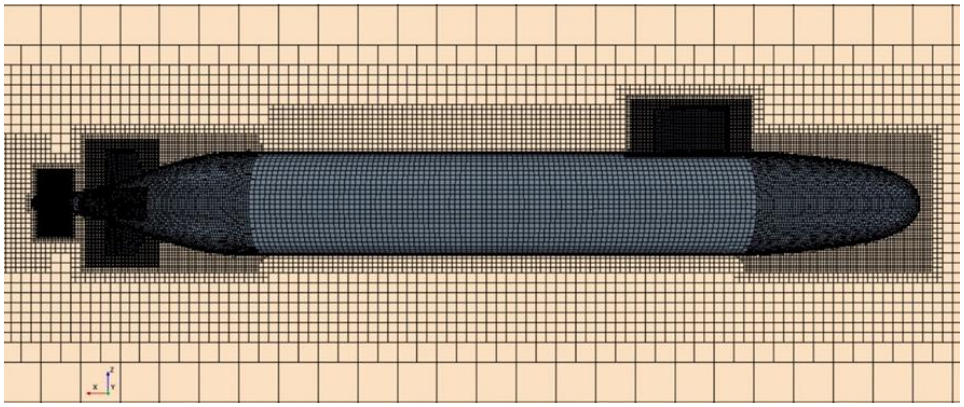


Fig. 8. Unstructured mesh layout for AFF-8 Suboff UV model cases

Furthermore, flow viscous effects from prototype model near wall in this work need to be taken into consideration for mesh refinement strategy in LRN region of Menter's k-ω SST mathematical turbulence model via boundary layer concept where flow velocity gradient normal to the wall varies dramatically (J.C.Date and S.R.Turnock, 1999; David C.Wilcox, 2006). The flow boundary layer development over a thin (Starting from zero thickness leading edge) flat plate surface will be elegantly illustrated as Fig. 9.

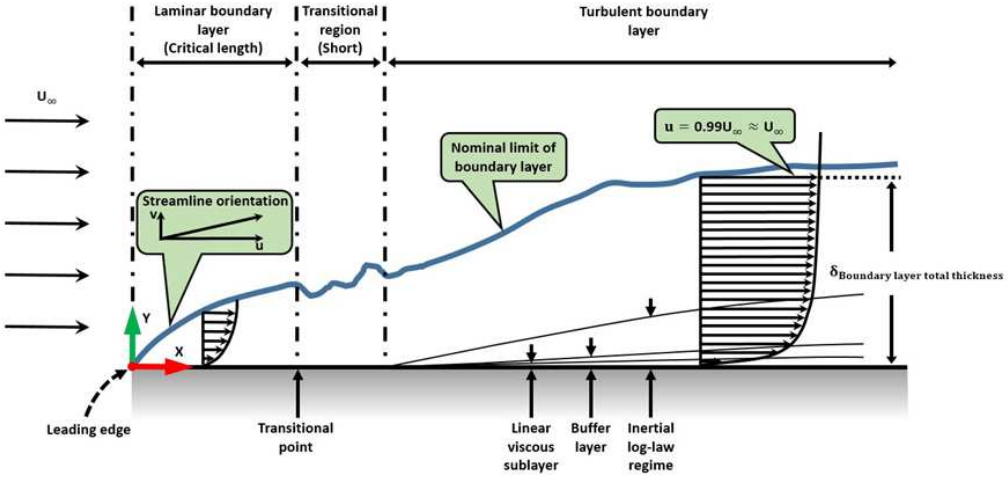


Fig. 9. Generic flow boundary layer development over a thin flat plate surface (Scale is exaggerated for clarity)

As depicted in Fig. 9, the undeveloped flow through leading edge is laminar at first surface region. Along with flow crossing, it becomes more and more turbulent in transitional region and ultimately turns into a turbulent flow (Cortana, 2013). The length of transitional region depends on flow velocity fluctuations and pressure distributions, wall shear stress, kinematic viscosity, fluid density and surface roughness (Maxim Candries, 2001). In this way, turbulent boundary layer can be piecewise hypothesized as linear viscous sublayer of inner layer, buffer layer of inner layer, inertial log-law regime of inner layer and outer layer, which is entirely presented as Fig. 10.

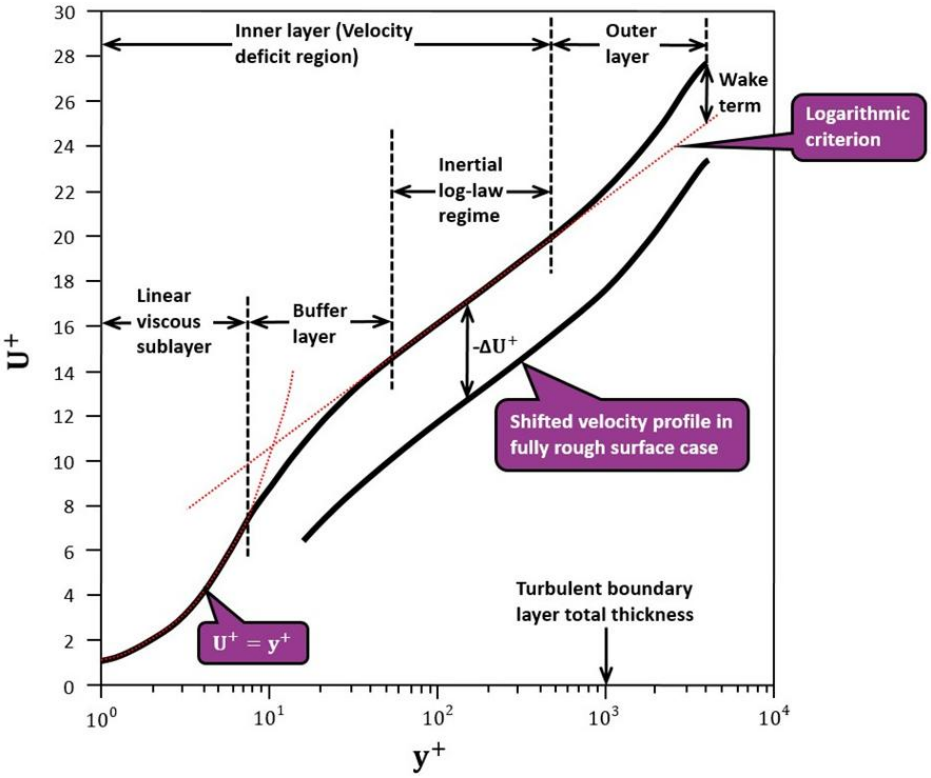


Fig. 10. Generic sub-regions of turbulent boundary layer and near wall treatment

In the sense of near wall flow physics, viscous effects are not dominant within inertial log-law regime while turbulence influences could be ignored within linear viscous sublayer. In buffer layer, fluid shear stress properties begin to deflect between viscous and turbulent (Hermann Schlichting, 1979). With regard to near wall treatment adopted in this paper, non-dimensional flow velocity profile U^+ is linear within viscous sublayer and in line with logarithmic criterion within log-law regime (Yigit Kemal Demirel et al., 2014; C. Liu et al., 2022), severally, as Eqs. (15) and (16).

$$U^+ = y^+ \tag{15}$$

$$U^+ = \frac{1}{\kappa}\ln\left(\frac{y^+}{1+k_s^+}\right) + B - \Delta U^+(k_s^+) \tag{16}$$

Where, y^+ represents non-dimensional normal distance from FVM grid centroid to model surface, as $y^+ = \rho y_{distance} u^*/\mu$, which will be deemed as a global parameter in fluid solver; $y_{distance}$ denotes normal distance from grid centroid to model surface; μ is dynamic viscosity; k_s^+ represents non-dimensional equivalent sand-grain roughness height with respect to roughness Reynolds number and boundary roughness correction; B denotes log-law intercept for hydraulically smooth wall; ΔU^+ is shifted roughness function causing non-dimensional flow velocity profile declining within inertial log-law regime as shown in Fig. 10, which needs to be obtained empirically with correction variable k_s^+; u^* represents frictional velocity, as $u^* = U/U^+ = \sqrt{\tau_{wall}/\rho}$; U denotes flow mean velocity; τ_{wall} is wall skin shear stress magnitude, as $\tau_{wall} = \rho C_f U_{freestream}^2/2$; $U_{freestream}$ represents far field freestream velocity.

For the sake of calculating empirical skin friction coefficient C_f and undetermined τ_{wall}, Reynolds number estimations and Granville skin friction correction (Paul S. Granville, 1989; Leo Victor Lazauskas, 2005) for turbulent boundary layer will be included in this work, as Eqs. (17) to (19).

$$Re_{0.75} = \frac{C_{0.75}\sqrt{V_A^2 + (0.75\pi n D)^2}}{\nu} \tag{17}$$

$$Re_L = \frac{\rho U_{freestream} L_{character}}{\mu} \tag{18}$$

$$C_f = 0.0776[\log_{10}(Re_x) - 1.88]^{-2} + 60Re_x^{-1} \tag{19}$$

Where, $Re_{0.75}$ denotes Reynolds number along chord of propeller blade at 0.75R, which will be heuristically employed for open water propeller analysis; V_A is propeller average advance velocity; n represents propeller rotation speed; Re_L denotes Reynolds number applied in Suboff UV simulations with radial character length $L_{character} = D_{max}$; Re_x represents $Re_{0.75}$ or Re_L.
In addition, peripherally linked to von Kármán's turbulence and skin friction theory (Theodore von Kármán, 1934), the heuristic consideration of Granville skin friction correction expressed in Eq. (19) is that low Reynolds viscous effects from turbulent irrotational interface are able to influence velocity defect factor of turbulent boundary layer and outer layer law, which seems to bring about precise and reasonable empirical skin friction coefficients for this paper.

2.6 Convergence study and uncertainty analysis

In accordance with GCI (Grid Convergence Index) recommended in ITTC guidelines (ITTC, 1999, 00. 7.5-03-01-04, 1999; ITTC, 2017, 03. 7.5-03-01-01, 2017), grid convergence study needs to be implemented in pre-processing MTO stage of each CFD simulation case by means of grid halving approach to seek corresponding optimum cell number and meshing base size with proper grid-refinement ratio r. On the basis of relevant empirical CFD research outcomes (Ismail B. Celik et al., 2008; Tahsin Tezdogan et al., 2015), grid-refinement ratio r is cautiously finalized as $\sqrt{2}$ to weaken numerical error effects from the other sources in convergence study and to restrict redundant simulation overhead for fine cases. Numerical solutions in compliance with fine, medium and coarse grid types are nominally denoted as u_{h_1}, u_{h_2} and u_{h_3} for convergence study of each simulation case in this work, which will be formulized into asymptotic form, as Eqs. (20) to (24).

$$r_{12} = \frac{h_2}{h_1} \tag{20}$$

$$r_{23} = \frac{h_3}{h_2} \tag{21}$$

$$\varepsilon_{12} = u_{h2} - u_{h1} \tag{22}$$

$$\varepsilon_{23} = u_{h3} - u_{h2} \tag{23}$$

$$R_C = \frac{\varepsilon_{12}}{\varepsilon_{23}} \tag{24}$$

Where, $h_1 < h_2 < h_3$ respectively denote meshing base size of fine, medium and coarse grid types; R_C represents convergence rate consisting of four possibilities (William L. Oberkampf and Christopher J. Roy, 2010):
1. Monotonic convergence: $0 < R_C < 1$
2. Oscillatory convergence: $-1 < R_C < 0$
3. Monotonic divergence: $R_C > 1$
4. Oscillatory divergence: $R_C < -1$

By contrast, convergence rate is supposed to be within narrow interval $0 < R_C < 1$ to ensure credibility and applicability of simulation solutions.
As to solution uncertainty analysis for each CFD simulation case in this paper, two errors need to be considered: discretization error and simulation error (Luıs Eca and Martin Hoekstra, 2006). Discretization error validation focuses on deviations between exact experimental result and corresponding discretization simulation solutions under aforementioned three grid types, which will be expressed as Eq. (25)

$$E = \delta_E - \delta_S = \delta_E - (\delta_{SM} + \delta_{SN}) \tag{25}$$

Where, δ_E denotes measurement error generated in experimental field test; δ_S represents simulation error; δ_{SM} is additive modeling error including model compatibility error, meshing error and detail modeling error; δ_{SN} denotes numerical error cumulated in entire CFD solving process, which is susceptible to finite precision of computer CPU, nonlinearity of governing equations in Menter's k-ω SST mathematical turbulence model and uncoupling between RANS momentum equations and corresponding transport equations.
According to Frederick Stern et al. (2001), the most primary source of error and uncertainty in CFD

investigations come from grid. With regard to governing equations in k-ω SST turbulence model, if discretization error $E(h)$ between a discretization simulation solution u and corresponding analytical solution u_a is proportional to meshing base size h within a tailored norm space $\|V\|$ as Eq. (26), the discretization simulation solution u can be deemed as p_fth-order accuracy (Philippe G. Ciarlet, 1978; LeVeque and Randall J, 2006).

$$E(h) = \|u - u_a\| = Ch^{p_f} + O\left(h^{(p_f+1)}\right) \approx Ch^{p_f} \tag{26}$$

Where, C represents an empirical constant, which is independent of h; p_f denotes formal order of accuracy, which is the exponent of lowest order term in discretization error (John C. Strikwerda, 2004).

Furthermore, generalized RE (Richardson extrapolation) method is adopted in this work to estimate RE simulation error δ_{RES} with $\hat{p}$th-order accuracy (Patrick J. Roache, 1998; Ismail B. Celik and Jun Li, 2004). In the sense of uncertainty analysis, observed order of accuracy $\hat{p}$ mirrors and quantifies both reliability metrics and asymptotic approximation rate from a discretization simulation solution of k-ω SST governing equations to corresponding analytical solution, which ought to be precisely hypothesized. On the basis of priori outcomes from convergence study, one-term estimation for RE simulation error δ_{RES} in regards to fine grid type case and corresponding observed order of accuracy $\hat{p}$ will be expressed in Eqs. (27) and (28).

$$\delta_{RES} = \frac{\varepsilon_{12}}{r^{\hat{p}}-1} \tag{27}$$

$$\hat{p} = \frac{\ln(\varepsilon_{23}/\varepsilon_{12})}{\ln(r)} \tag{28}$$

Where, $\hat{p} > 0$ indicates that discretization simulation solutions are monotonically convergent.

For the sake of solution uncertainty analysis under three grid type nodes, FS (Factor of Safety) approach (Tao Xing and Frederick Stern, 2009) seems to be more reasonable and applicable with proper overall conservativeness and less metrics scatter in contrast to GCI, CF (Correction Factor) or even LSQ (Least Squares) approaches, which will be employed in this paper to finalize both FS uncertainty estimator U_{FS} and FS discretization error estimator E_{FS}, as Eqs. (29) to (31).

$$U_{FS} = \begin{cases} [FS_1 P_n + FS_0(1 - P_n)]|\delta_{RES}|, 0 < P_n \leq 1 \\ [FS_1 P_n + FS_2(P_n - 1)]|\delta_{RES}|, P_n > 1 \end{cases} \tag{29}$$

$$P_n = \frac{\hat{p}}{p_f} \tag{30}$$

$$E_{FS} = P_n|E(h)| \tag{31}$$

Where, FS_0, FS_1 and FS_2 are flexible tuning parameters; P_n represents normalized order of accuracy, which needs to be bound with FS_0, FS_1 and FS_2 to characterize solution convergence degree in formal order of accuracy independent manner.

In addition, EUEI (Equivalent uncertainty effectivity index) Ψ_{L_2} (Tyrone S. Phillips and Christopher J. Roy, 2014) will be included in this research, which is expressed as Eq. (32).

$$\Psi_{L_2} = \frac{U_{FS}}{\|E_{FS}\|_{L_2}} = \frac{U_{FS}}{\sqrt{\frac{1}{3}\sum_{i=1}^{3} E_{FS_i}^2}} = \frac{U_{FS}}{\sqrt{\frac{1}{3}\sum_{i=1}^{3} [P_n|E(h)|]_i^2}} \tag{32}$$

Where, L_2 denotes L_2-norm computation under three grid type nodes: fine, medium and coarse.

In fact, the closer EUEI Ψ_{L_2} approaches one, the more conservative uncertainty estimator will be with negligible discretization error and the more accurate simulation solution will be with credible fine grid type.

3. Numerical methodology

3.1 Open water propeller analysis

The nomenclature open water indicates one status where an isolated propeller is not obstructed by appendages and fully exposed into surrounding water. As for INSEAN E1619 propeller investigated in this work, MRF method will be adopted for model-scale open water propeller analysis, which could show satisfactory performance if there is few wake interference around the propeller (Dmitriy

Ponkratov and Constantinos Zegos, 2015). In this way, E1619 propeller model will steadily rotate within rotation region in entire CFD simulation process with uniform inlet flow to simulate realistic single phase operating circumstance of open water propeller field test.

By convention, an essential purpose of open water propeller analysis is to validate intrinsic open water characters of the propeller with respect to dimensionless amplified open water torque coefficient $10K_{QO}$, open water thrust coefficient K_{TO} and open water propeller efficiency η_O in compliance with EFD OWC data (Sinan Burunsuz et al., 2017; Tran Ngoc Tu, 2019), which can be expressed from Eqs. (33) to (36).

$$10K_{QO} = \frac{10Q_O}{\rho n^2 D^5} \tag{33}$$

$$K_{TO} = \frac{T_O}{\rho n^2 D^4} \tag{34}$$

$$\eta_O = \frac{JK_{TO}}{2\pi K_{QO}} = \frac{V_A K_{TO}}{2\pi n D K_{QO}} = \frac{V_A T_O}{2\pi n Q_O} \tag{35}$$

$$J = \frac{V_A}{nD} \tag{36}$$

Where, Q_O represents open water propeller torque; T_O denotes open water propeller thrust; J is propeller advance coefficient, which varies within interval [0.2, 1.1] for both EFD and CFD cases.

3.2 Straight-ahead resistance simulation

On the foundation of Newton's second law, there are two primary forces acting on straight-ahead navigating vehicle, namely, stress and shear stress. In this way, dimensionless pressure and skin friction coefficient distributions need to be obtained in this work along upper meridian line of AFF-1 and AFF-8 model contours to validate and investigate the underwater velocity-pressure development characteristics of DARPA Suboff models (Mojtaba Maali Amiri, 2018; Dong Li et al., 2021), which is depicted as Fig. 11.

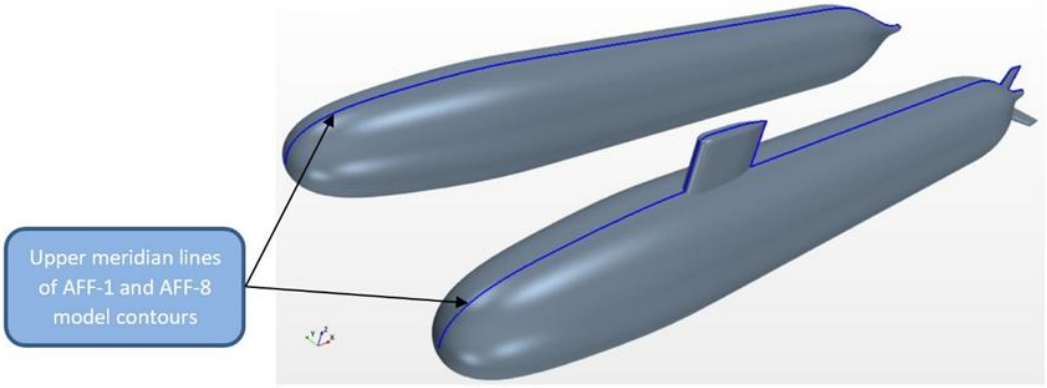


Fig. 11. Upper meridian line of AFF-1 and AFF-8 model contours

In addition, average development distribution of wake stream-wise velocity profile is an indispensable aspect in straight-ahead resistance simulation, as well. In contrast with EFD results and previous empirical comparison CFD outcomes (Nathan Chase, 2012; Bhushan Shanti et al., 2013; Liwei Liu et al., 2018; Chunyu Guo et al., 2023), six straight-ahead wake stream-wise velocity profile cases will be implemented for both AFF-1 and AFF-8 at three tailored piecewise stern plane locations with uniform inlet flow to correspondingly capture and analyze more subtle velocity details of non-uniform wake development distributions.

3.3 Self-propulsion simulation

With regard to designing and hydrodynamic pre-testing for vehicle-propeller, self-propulsion interaction performance assessment is one crux. In this paper, two backbone methods for self-propulsion simulation are about to be put forward and contrastively applied to model stern self-

propulsion propeller and to estimate self-propulsion interaction performance between DARPA Suboff vehicle and INSEAN E1619 propeller, namely, body force method and full geometric model method. In accordance with body force theorem (Vladimir I. Krasilnikov, 2013), the virtual actuator disk instead of real self-propulsion E1619 propeller model needs to be placed at stern propeller mounted plane location for both AFF-1 and AFF-8 Suboff UV models, which will be presented as Fig. 12.

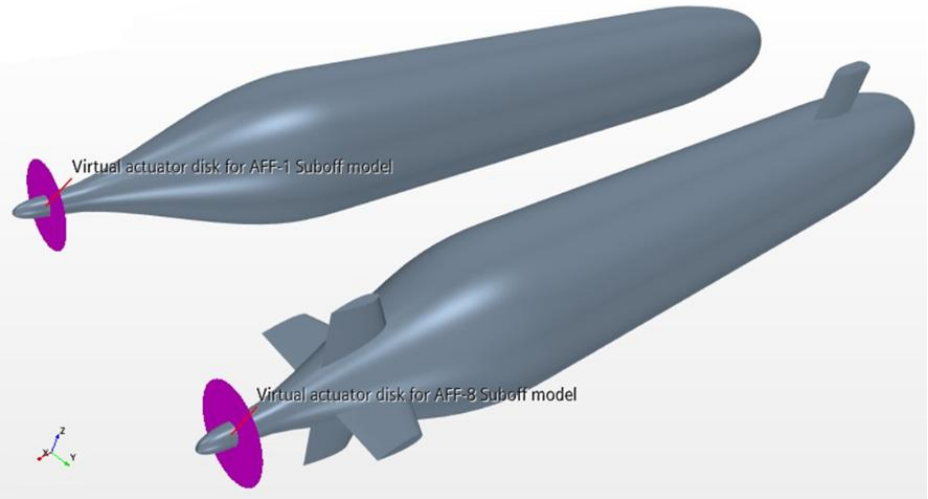


Fig. 12. Virtual actuator disk for both AFF-1 and AFF-8 Suboff UV models

As for E1619 propeller in body force method, intrinsic open water characters, equivalent geometry, elemental thrust and torque distributions within body fixed frame, inlet flow features, propeller rotation direction rule and propeller rotation speed need to be duplicated and redefined in corresponding virtual actuator disk, which is able to replace original propeller by means of an infinite number of propeller blades (Yan Naing Win et al., 2013). In this way, self-propulsion interaction effects between Suboff vehicle and E1619 propeller can be explicitly estimated via body force method under different initial or boundary conditions.

Similar to body force method, Suboff UV models in full geometric model method will nominally navigate forward thrust by full geometric E1619 propeller model at a certain rotation speed while inlet flow is requisite to complete this relative self-propulsion motion. Inevitably, total resistance acting on vehicle and propeller models within simulation initial stage would increase dramatically on account of viscous damping force, pressure, skin friction, vortices or turbulent boundary layer effects. As a result, self-propulsion vehicle velocity (Inlet flow velocity relatively towards the UV) and propeller rotation speed need to be tuned cooperatively until E1619 propeller thrust is nearly identical with vehicle total resistance along forward orientation, which is called net force balance. In compliance with thrust identity method (Cihad Delen et al., 2017; Yung An Chu et al., 2018), if net force balance approaches zero, corresponding UV self-propulsion point will be achieved.

In addition, certain self-propulsion performance particulars in regard to relative rotation efficiency η_r, dimensionless amplified self-propulsion torque coefficient $10K_{QS}$, self-propulsion thrust coefficient K_{TS}, hull efficiency η_h, propulsion efficiency η_d, ideal propeller efficiency η_i, effective power P_e and propeller delivered power P_d (Alexander B Phillips et al., 2008; ITTC, 2014, 00. 7.5-03-03-01, 2014) are expressed from Eqs. (37) to (44), which will be numerically investigated in section 4.4.

$$\eta_r = \frac{Q_O}{Q_S} \tag{37}$$

$$10K_{QS} = \frac{10Q_S}{\rho n^2 D^5} \tag{38}$$

$$K_{TS} = \frac{T_S}{\rho n^2 D^4} \tag{39}$$

$$\eta_h = \frac{1-t_M}{1-w_T} \quad (40)$$

$$\eta_d = \eta_r \eta_h \eta_O \quad (41)$$

$$\eta_i = \frac{2}{1+\sqrt{1+C_{T_h}}} \quad (42)$$

$$P_e = R_T V_S \quad (43)$$

$$P_d = \frac{P_e}{\eta_d} \quad (44)$$

Where, Q_S represents self-propulsion propeller torque; T_S denotes self-propulsion propeller thrust; t_M is thrust deduction factor as $t_M = 1 - R_T/T_S$; R_T represents vehicle total resistance along forward orientation; w_T denotes nominal wake coefficient, which can be derived from average development distribution of wake stream-wise velocity profile, as $w_T = 1 - V_A/V_S$; V_S is self-propulsion vehicle velocity; C_{T_h} represents thrust loading factor in momentum lemma (Volker Bertram, 2000), as $C_{T_h} = T_S/(\rho V_A^2 D^2 \pi/8)$.

4. Result presentations and discussions

In this paper, pre-processing MTO study, open water propeller analysis, straight-ahead resistance simulation and self-propulsion simulation have been elaborately carried out with plentiful pre-processing MTO study outcomes and CFD simulation results, which are about to be spread out and discussed respectively for further probable improvements.

4.1 Pre-processing MTO study

On the basis of GCI recommendations and relevant ITTC guidelines, grid convergence study and solution uncertainty analysis have been executed in pre-processing MTO stage of open water, straight-ahead and self-propulsion cases correspondingly with credible, reasonable and applicable meshing base size and cell number, which will be listed in Table 3.

Table 3

Meshing base size and cell number for grid convergence study and solution uncertainty analysis.

		Open water propeller analysis		AFF-1 straight-ahead resistance simulation		AFF-8 straight-ahead resistance simulation		AFF-8 self-propulsion simulation	
#	Grid type	Meshing base size [m]	Cell number [-]	Meshing base size [m]	Cell number [-]	Meshing base size [m]	Cell number [-]	Meshing base size [m]	Cell number [-]
I	Fine	0.083916	552931	0.022337	933367	0.024459	1157652	0.024459	2147527
II	Medium	0.118676	368550	0.031589	406419	0.034589	530917	0.034589	1217707
III	Coarse	0.167833	260180	0.044674	192139	0.048918	238093	0.048918	770599

As summed in Table 3, based upon grid halving approach, meshing base size in each case increase piecewise from fine to coarse grid type with grid-refinement ratio $r = \sqrt{2}$. In this work, propeller advance coefficient J is uniformly considered as 0.2081 in open water convergence study and uncertainty analysis while freestream velocities for AFF-1 straight-ahead case and AFF-8 cases are severally predetermined as $3.046 m/s$ and $2.75 m/s$. Consequently, Reynolds numbers for open water case, AFF-1 straight-ahead case and AFF-8 cases are able to be estimated from Eqs. (17) or (18), as 20574, 938569 and 847362, respectively. In this way, prism layer total thickness, meshing base size and cell number can be correlatively finalized for fine, medium and coarse grid type cases in each convergence study and uncertainty analysis to ensure a smooth computational volume transition between last prism grid layer and core volumetric mesh mentioned in section 2.5. Moreover, different computational flow domain scale and local mesh refinements for appendages or propeller blades may contribute to the cell number uptrend of open water, straight-ahead and self-propulsion cases.

Furthermore, on the foundation of grid halving approach, discretization error methodology, FS

approach and generalized RE method, percentage of quasi-SSE, convergence rate R_C, observed order of accuracy $\hat{p}$ and EUEI Ψ_{L_2} for open water, straight-ahead and self-propulsion cases have been presented in Table 4.

Table 4
Particulars and results for grid convergence study and solution uncertainty analysis.

GCI_{Fine} criteria for I II III	Open water propeller analysis	AFF-1 straight-ahead resistance simulation	AFF-8 straight-ahead resistance simulation	AFF-8 self-propulsion simulation
Percentage of quasi-SSE [%]	1.3972325	0.5372311	0.4595164	2.0236086
Convergence rate R_C [-]	0.3308803	0.2963507	0.4570893	0.3647963
Observed order of accuracy $\hat{p}$ [-]	3.1912369	3.5092452	2.2589042	2.909674
EUEI Ψ_{L2} [-]	1.1872518	1.1536026	1.3475173	1.4750231

As to self-propulsion uncertainty analysis, available experimental OWCs in (Alejandro M. Castro et al., 2011) with a fully predictive methodology can be employed as EFD data in this paper. Hence, dimensionless amplified open water torque coefficient $10K_{QO}$, vehicle total resistance along forward orientation R_T and amplified self-propulsion torque coefficient $10K_{QS}$ are correspondingly adopted as discretization simulation solution in open water, straight-ahead and self-propulsion uncertainty analyses. In general, discretization simulation solutions for three grid type cases in uncertainty analysis are not fully convergent in contrast with EFD data, which can be validated and quantified by means of percentage of quasi-SSE. Besides, in the light of cell number condition and one-term estimation manner of generalized RE method, fine grid type would be employed as optimum grid type for each uncertainty analysis.
As shown in Table 4, due to an order of magnitude discrepancy between $10K_Q$ and R_T, percentage of quasi-SSE for open water and self-propulsion cases are obviously higher than straight-ahead cases. R_C of four cases are all within acceptable monotonic convergence interval (0, 1) as expected. In addition, R_C and $\hat{p}$ of AFF-8 straight-ahead case are relatively inferior to the others, which seems to be brought about by great order of magnitude of corresponding discretization simulation solutions and AFF-8 appendage resistance influences. With regard to uncertainty estimation, $\hat{p}$ and Ψ_{L_2} of open water case and AFF-1 straight-ahead case are definitely better than AFF-8 cases, which indicates that reliability metrics and asymptotic approximation rate of discretization simulation solutions in open water and AFF-1 straight-ahead case with overall conservativeness and metrics scatter in corresponding uncertainty estimator are generally superior to AFF-8 cases. In this work, abrupt and sharp model surface changing in component intersections and training edge of propeller blades and UV appendages, larger computational flow domain scale or self-propulsion interaction effects might contribute to highest uncertainty in AFF-8 self-propulsion case.

4.2 Open water propeller analysis

In accordance with pre-processing MTO study outcomes and MRF method, open water propeller analysis for isolated E1619 propeller model has been carried out and validated via INSEAN open water EFD data. For the purpose of fair validation and comparison, EFD OWCs, CFD OWCs in this paper and previous empirical comparison CFD OWCs obtained from (Liwei Liu et al., 2021) and with twelve operating points are plotted in Fig. 13.

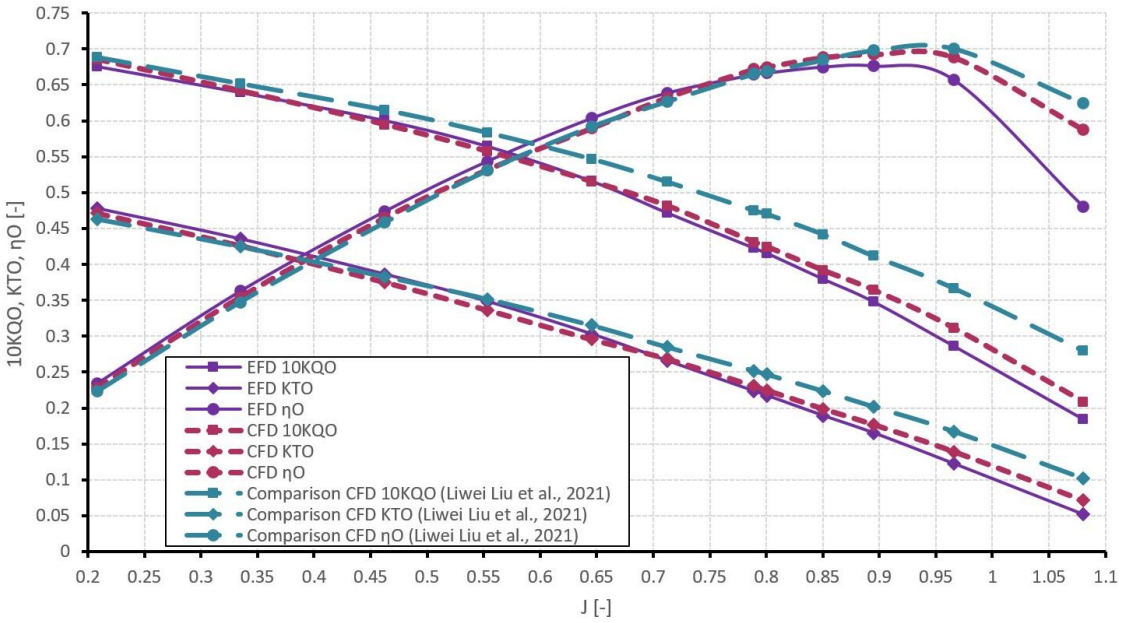


Fig. 13. OWC results of open water propeller analysis for INSEAN E1619 propeller model

In regards to CFD OWCs estimated in this paper, E-N (Experimental-Numerical) relative errors of $10K_{QO}$, K_{TO} and η_O curves are all below 4% with slightly fluctuation in $J \leq 0.8005$ and rise significantly in $J > 0.8005$, especially for K_{TO} curve, which seems to arise from experimental limitations or algorithm stability of MRF method under high propeller rotation speed circumstance. Besides, in $J < 0.6458$ and $J > 0.8505$, most E-N relative errors of CFD OWCs in this paper are correspondingly lower than comparison CFD errors, which may be benefit from abundant pre-processing MTO studies. In general, MRE (Mean Experimental-Numerical relative error) of $10K_{QO}$, K_{TO} and η_O curves estimated in this work and comparison CFD $10K_{QO}$, K_{TO} and η_O curves are 3.3059%, 7.0152%, 3.8626%, 13.7498%, 18.2674% and 5.0212%, respectively, which indicates that CFD OWC results for E1619 propeller model in this work are more accurate than comparison CFD OWC results and fairly satisfying except in $J > 0.8005$.

4.3 Straight-ahead resistance simulation

As a pre-validation simulation, vehicle total resistance along forward orientation R_T is necessary to be estimated for both AFF-1 and AFF-8 models on the basis of pre-processing MTO studies. Initial inlet flow velocities V_I of two Suboff model cases have been individually predetermined as eight operating points from $2.75m/s$ to $9.255m/s$. EFD total resistance curves (Han-Lieh Liu and Thomas T. Huang, 1998), CFD total resistance curves in this work and comparison CFD total resistance curves (Liwei Liu et al., 2021) are depicted in Figs. 14 and 15.

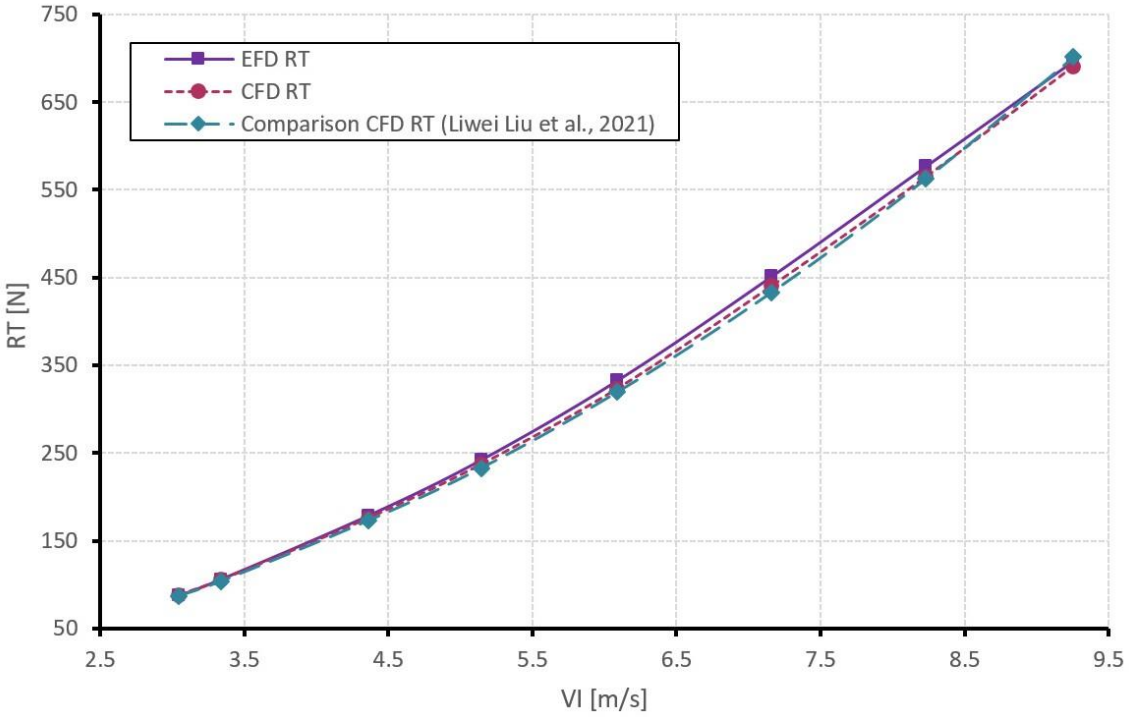


Fig. 14. Three total resistance curves for AFF-1 Suboff model

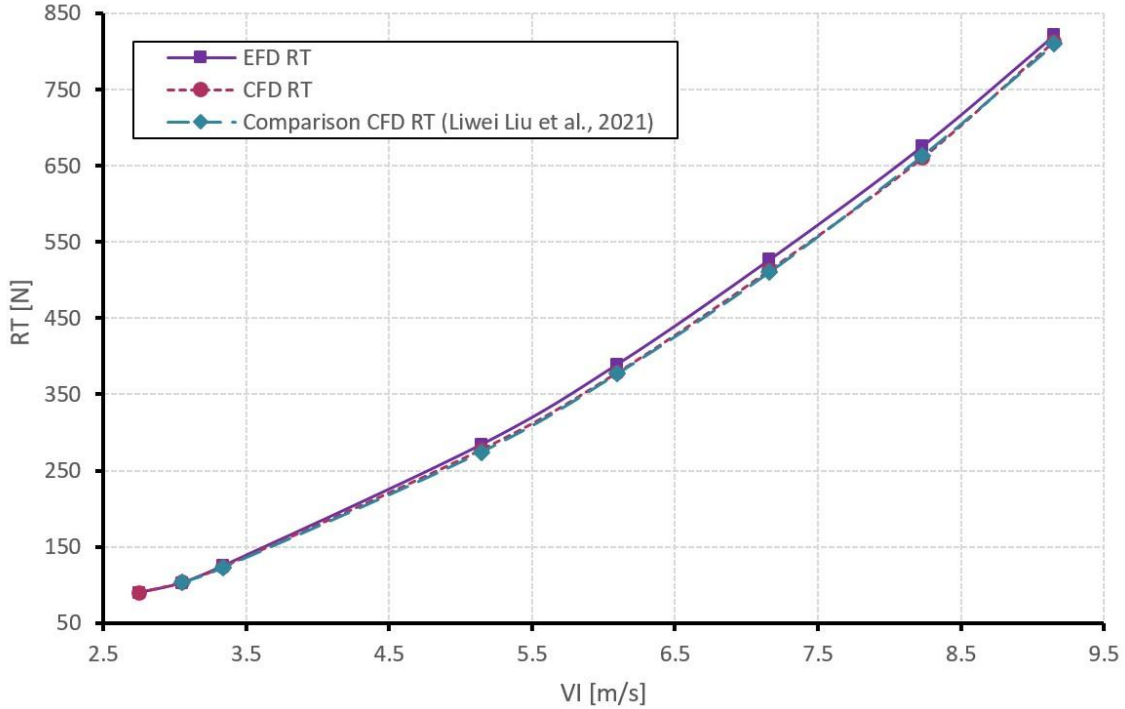


Fig. 15. Three total resistance curves for AFF-8 Suboff model

From Figs. 14 and 15, it can be explicitly found that comparison CFD total resistance curves and CFD total resistance curves in this work are both in line with EFD total resistance curves well in general for two Suboff UV models while orders of magnitude for entire AFF-8 total resistance results are correspondingly higher than AFF-1 cases due to AFF-8 appendage resistance influences. In contrast to comparison CFD cases, E-N relative errors of total resistance results estimated in this work are all below 3% with a reasonable and steady trend. Furthermore, RMSE (Root mean square Experimental-Numerical relative errors) with respect to AFF-1 total resistance result estimated in

this work, AFF-1 comparison CFD total resistance result, AFF-8 total resistance result estimated in this work and AFF-8 comparison CFD total resistance result have been respectively acquired as 1.8845%, 2.9559%, 1.8465% and 2.3242%, which can be accepted within expected error tolerance. For the sake of vehicle model detail validation and flow velocity-pressure development characteristics investigation, dimensionless pressure and skin friction coefficient distributions along upper meridian line of AFF-1 and AFF-8 model contours are imperative to be estimated in straight-ahead resistance simulation, which will be presented severally from Figs. 16 to 18 with accessible experimental distribution data (Nancy C. Groves et al., 1989; Thomas T. Huang et al., 1989; Han-Lieh Liu and Thomas T. Huang, 1998) and comparison CFD distribution curves (Chi Yang and Rainald Löhner, 2003; Niklas Alin et al., 2010; Liwei Liu et al., 2021; Dong Li et al., 2021; Jingyuan Li et al., 2021). Initial inlet flow velocity in this paper match EFD and comparison CFD cases uniformly as $V_I = 3.34 m/s$ for fair validation and comparison.

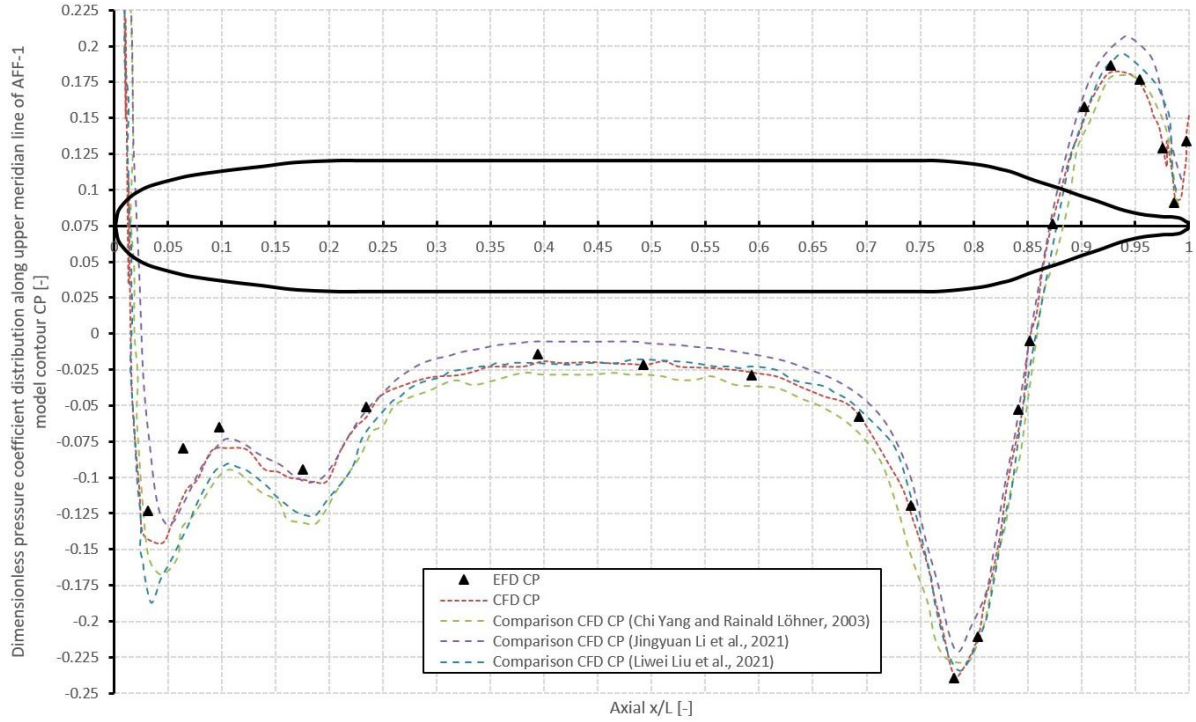


Fig. 16. Dimensionless pressure coefficient distribution along upper meridian line of AFF-1 model contour

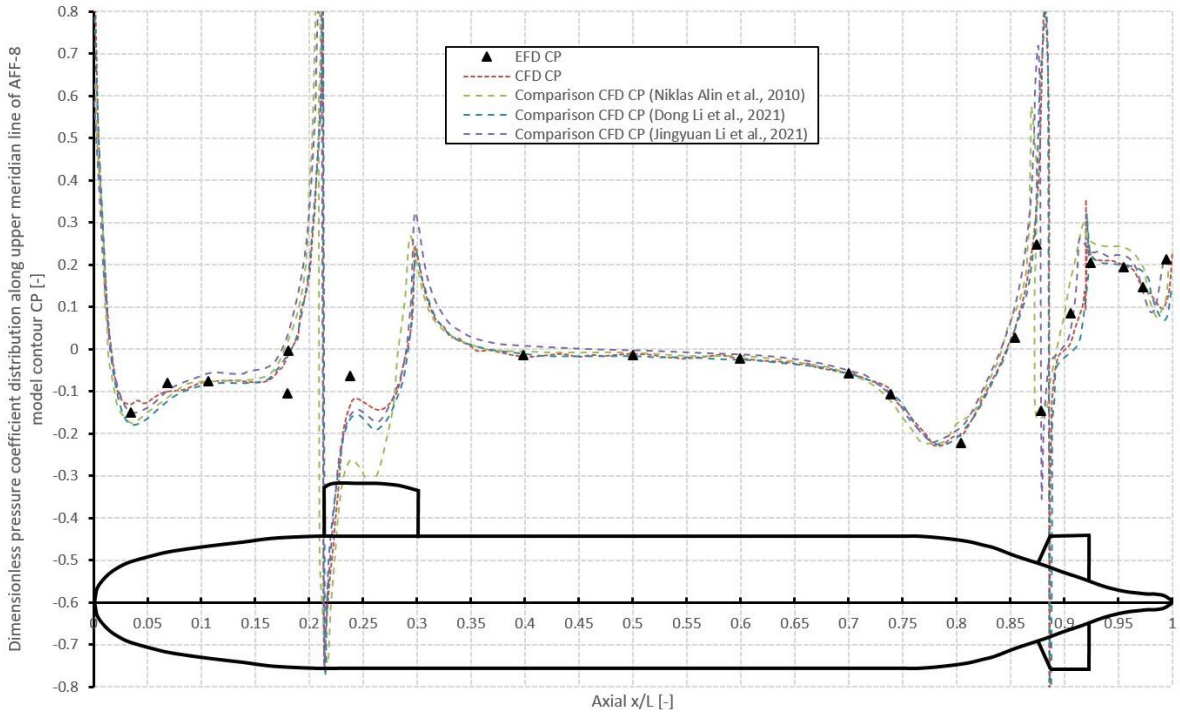
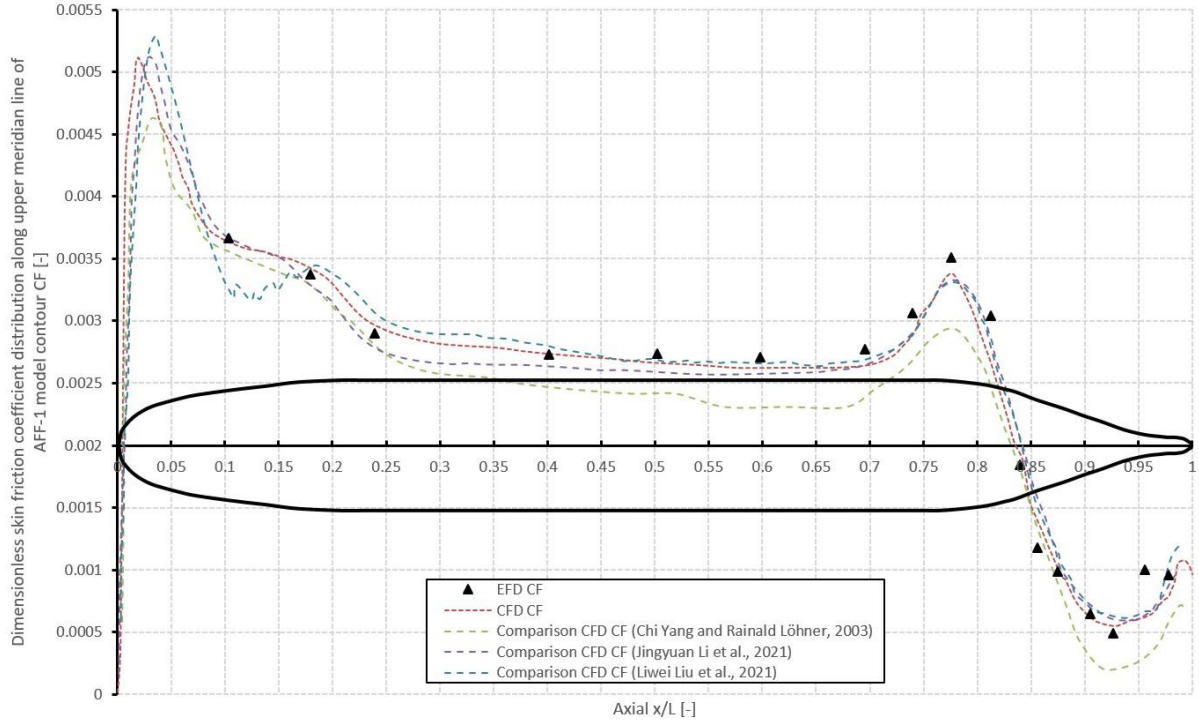


Fig. 17. Dimensionless pressure coefficient distribution along upper meridian line of AFF-8 model contour



1111

Fig. 18. Dimensionless skin friction coefficient distribution along upper meridian line of AFF-1 model contour

As illustrated from Figs. 16 to 18, E-N relative error of CFD pressure coefficient meridian distribution for AFF-1 model is much lower than that of pressure distribution for AFF-8 model and skin friction distribution for AFF-1 model in general. All CFD distribution curves meet huge bounded fluctuations in axial $x/L < 0.3$ and axial $x/L > 0.7$, which reflects abrupt and sharp model surface changing and dramatic local force variation in bow and stern region of Suboff UV. By contrast, CFD pressure distribution curves for both AFF-1 and AFF-8 models estimated in this paper are steadier in axial $x/L < 0.15$ than the other comparison CFD curves with slightly lower

overall average validation deviations. Except in axial $x/L < 0.27$ and axial $x/L > 0.85$, E-N relative error of CFD pressure distribution curve for AFF-8 model estimated in this paper and corresponding comparison CFD curve (Dong Li et al., 2021) are generally identical and achieve minimum in axial $x/L < 0.76$ and axial $x/L > 0.45$. In addition, obviously, overall average validation deviation of CFD skin friction distribution curve estimated in this paper is lower than the other comparison CFD curves, which seems to be benefit from vehicle model detail optimizations or local mesh refinements.

Against straight-ahead navigation orientation, average development distributions of wake stream-wise velocity profile have been depicted in contrast with EFD investigations (Nathan Chase, 2012) and comparison CFD studies (Bhushan Shanti et al., 2013; Liwei Liu et al., 2021; Chunyu Guo et al., 2023) at three tailored piecewise stern plane locations $x/L = 0.978$ (Propeller mounted plane), 1.04 and 1.2 for both AFF-8 and AFF-1 Suboff UV models with uniform inlet flow velocity $V_I = 2.75m/s$, as Figs. 19 to 22.

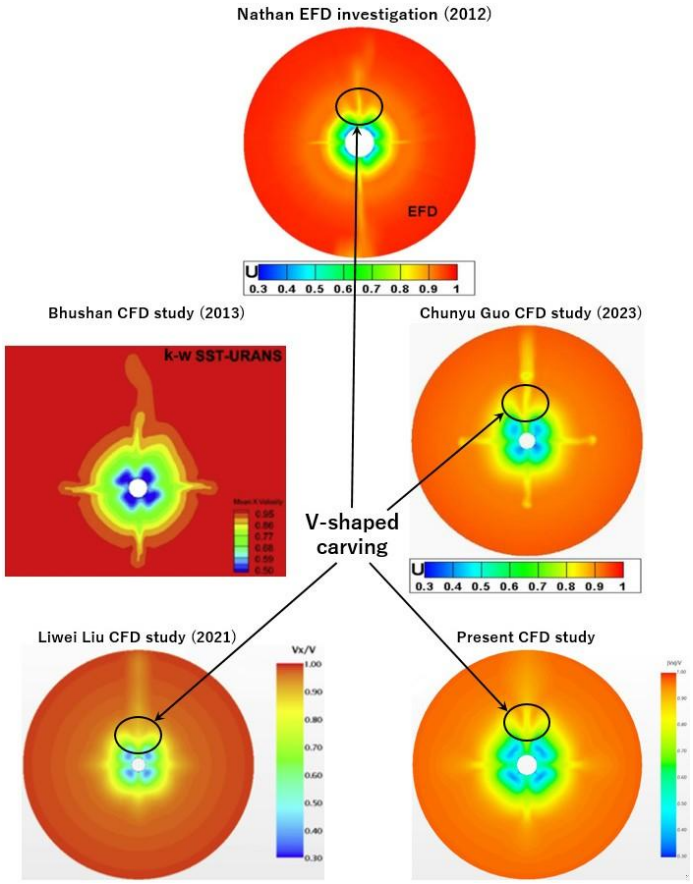


Fig. 19. EFD, three comparison CFD and present CFD wake velocity profile distributions at propeller mounted plane ($x/L = 0.978$) for AFF-8 model

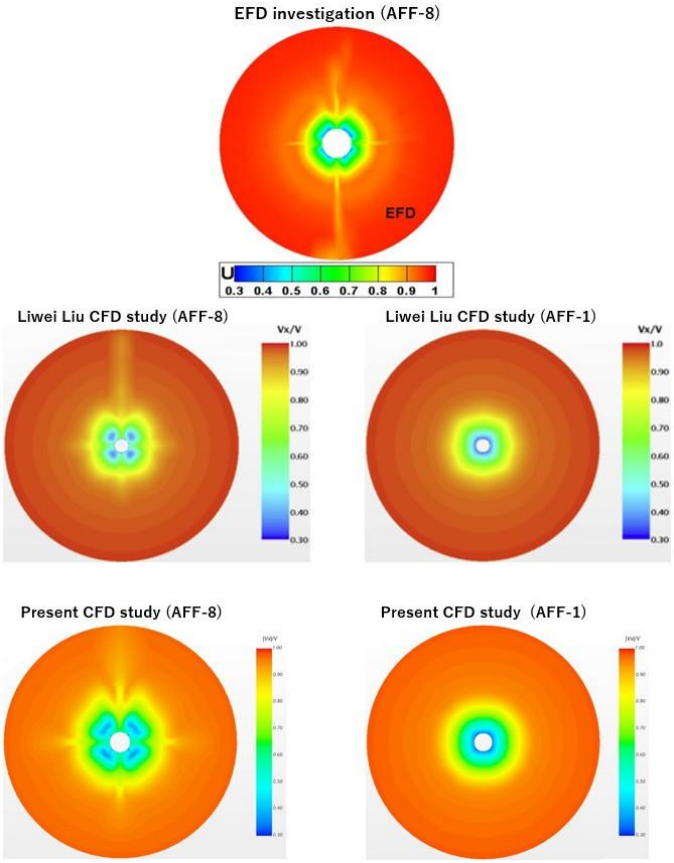


Fig. 20. EFD, Liwei Liu comparison CFD and present CFD wake velocity profile distributions at stern plane location $x/L = 0.978$ for both AFF-8 and AFF-1 models

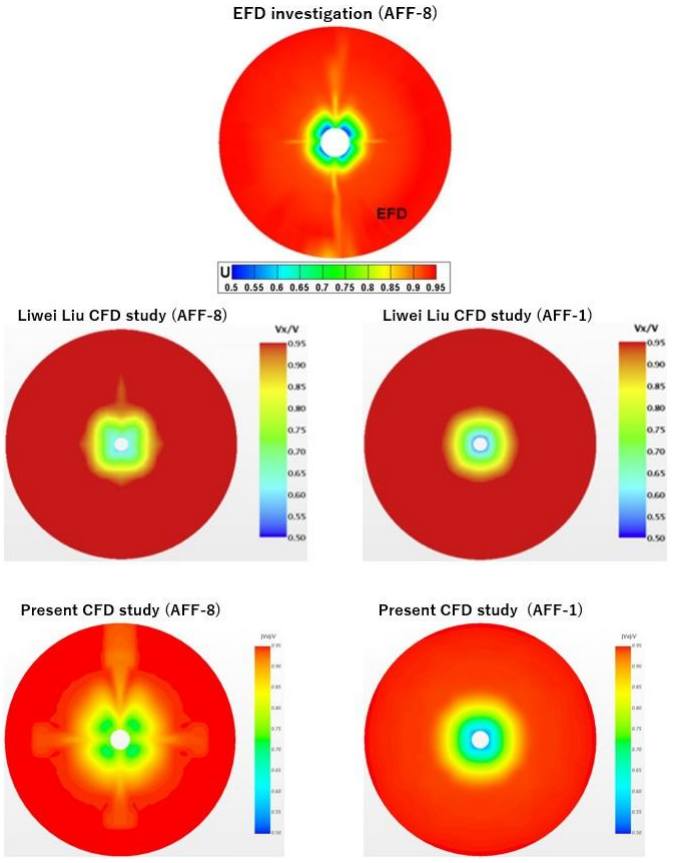


Fig. 21. EFD, Liwei Liu comparison CFD and present CFD wake velocity profile distributions at stern plane location $x/L = 1.04$ for both AFF-8 and AFF-1 models

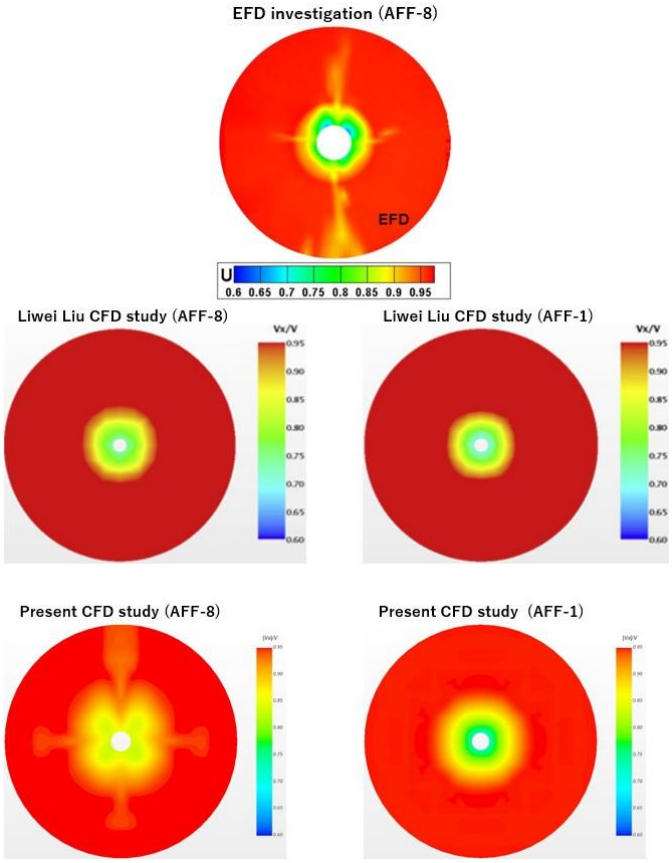


Fig. 22. EFD, Liwei Liu comparison CFD and present CFD wake velocity profile distributions at stern plane location $x/L = 1.2$ for both AFF-8 and AFF-1 models

As summed from Figs. 19 to 22, EFD, three comparison CFD and present CFD wake velocity profile distributions at propeller mounted plane ($x/L = 0.978$) for AFF-8 model are all non-uniform and irregular while AFF-1 wake velocity profile distributions are much more radially symmetric than corresponding AFF-8 cases. Explicitly, except far field depleted area, bare hull with vehicle appendage have contributed a dominant effect on average development distributions of downstream wake velocity profiles. Moreover, V-shaped carving of AFF-8 wake velocity profile distribution at propeller mounted plane in this work shows acceptable agreement with EFD investigations, Chunyu Guo comparison CFD study and Liwei Liu comparison CFD study with slightly sharper V-shape angle and moderate stern fin training edge contour rather than obscure V-shaped carving in Bhushan comparison CFD study. In fact, downstreaming through vehicle sail or stern fins, the boundary layer gets thinner rapidly and becomes thicker on the side of corresponding depleted region, which slightly accelerates wake velocity near V-shaped carving area. From stern plane location $x/L = 0.978$ to $x/L = 1.2$, wake velocity contour lines of three AFF-1 cases and three AFF-8 cases correspondingly become more and more obscure with a velocity rising trend as Figs. 20 to 22, which seems to indicate that influences from bare hull, vehicle appendage and boundary layer along downstream orientation ($x/L = 0.978$, 1.04 and 1.2) are fading out step by step and wake stream-wise velocity far away from propeller mounted plane becomes more and more identical up to uniform freestream velocity.

4.4 Self-propulsion simulation

For the sake of hydrodynamic interaction effect investigation between Suboff UV and E1619 propeller which have been individually validated and investigated from section 4.1 to 4.3, self-propulsion simulations need to be conducted for both AFF-1 and AFF-8 self-propulsion models to

seek self-propulsion points using thrust identity method. Analogous to straight-ahead resistance simulation, eight suites of net force balance verification simulations with corresponding predetermined self-propulsion vehicle velocities from 2.75m/s to 9.255m/s are deemed as eight operating points in thrust identity method and self-propulsion point in each operating point with relevant propeller rotation speed, self-propulsion vehicle velocity and net force will be achieved if the net force acting on self-propulsion Suboff UV along forward orientation approaches zero. In this way, according to body force method and full geometric model method, self-propulsion point verification results for both AFF-1 and AFF-8 self-propulsion models in contrast with comparison CFD results (Liwei Liu et al., 2021) have been respectively plotted in Figs. 23 and 24.

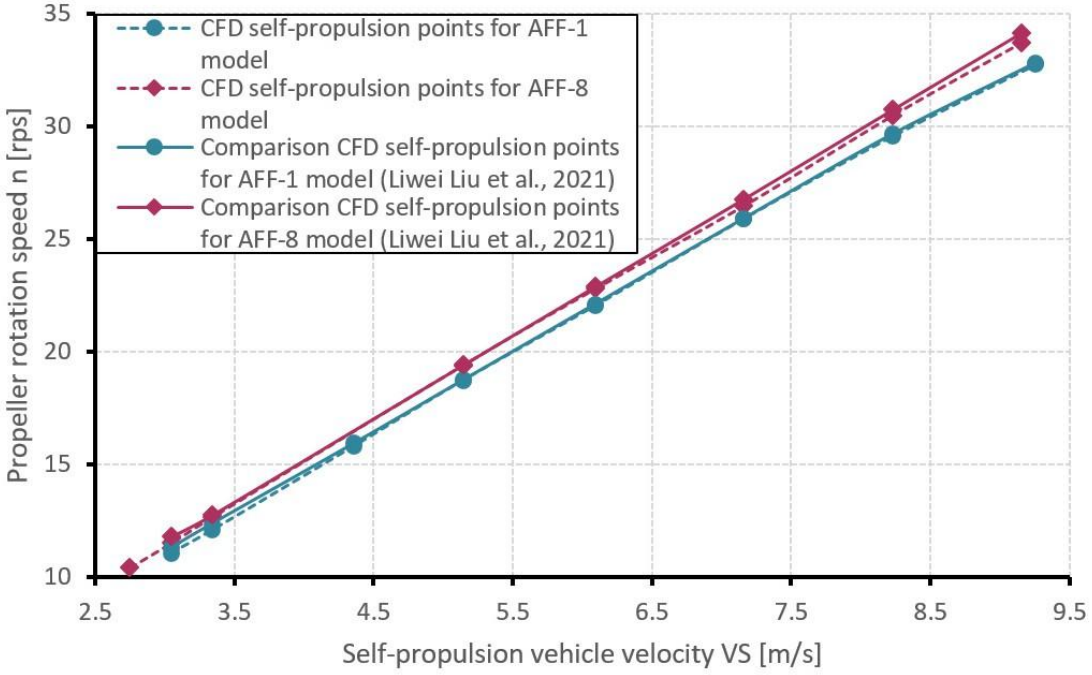


Fig. 23. Self-propulsion point verification results according to body force method

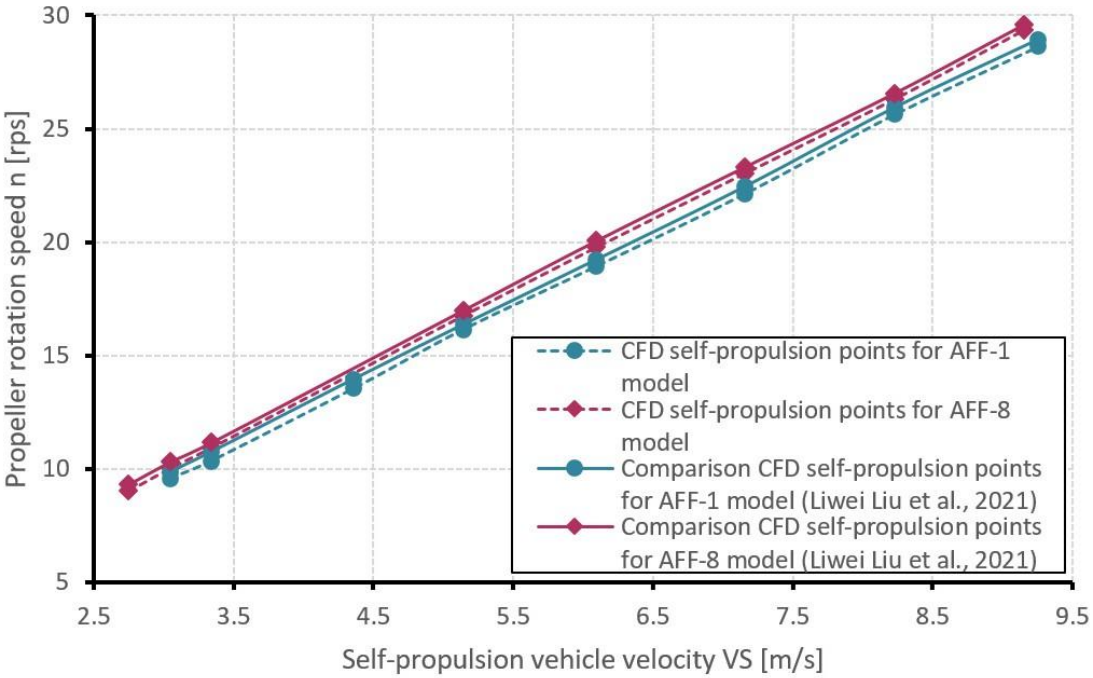


Fig. 24. Self-propulsion point verification results according to full geometric model method

As expected, distribution of each self-propulsion point verification results illustrated in Figs. 23 and 24 can be approximately treated as quasilinear. By intuitive contrast, with identical self-propulsion vehicle velocity, relevant propeller rotation speed acquired from full geometric model method is correspondingly lower than that of body force method, which seems to indicate that full geometric model method is more precise and promising for self-propulsion point estimation. In general, with identical propeller rotation speed, relevant self-propulsion vehicle velocity for AFF-8 case is correspondingly lower than that of AFF-1 case, which arises from AFF-8 appendage resistance influences. Furthermore, with identical self-propulsion vehicle velocity, relevant propeller rotation speed acquired in this paper is correspondingly lower than that of comparison CFD results, which might be benefit from abundant pre-processing MTO studies.

In the light of self-propulsion propeller modeling method comparison and further self-propulsion interaction performance assessment between DARPA Suboff vehicle and INSEAN E1619 propeller, crucial self-propulsion performance particulars on the basis of Eqs. (37) to (44) from section 3.3 for both AFF-1 and AFF-8 self-propulsion models have been numerically estimated in the framework of six predetermined baseline self-propulsion points, which are listed in Table 5 and 6.

Table 5

Self-propulsion performance particulars for AFF-1 self-propulsion model.

	V_S = 3.046 m/s			V_S = 5.144 m/s			V_S = 6.091 m/s			V_S = 7.161 m/s			V_S = 8.231 m/s			V_S = 9.255 m/s		
Self-propulsion propeller modeling methods	Body force	Full geometric model	Comparison CFD OWCs	Body force	Full geometric model	Comparison CFD OWCs	Body force	Full geometric model	Comparison CFD OWCs	Body force	Full geometric model	Comparison CFD OWCs	Body force	Full geometric model	Comparison CFD OWCs	Body force	Full geometric model	Comparison CFD OWCs
J [-]	0.8994	0.8137	0.8137	0.9124	0.8226	0.8226	0.9153	0.8259	0.8259	0.9197	0.8294	0.8294	0.9232	0.8315	0.8315	0.9275	0.8348	0.8348
ηO [-]	-	0.6713	0.6756	-	0.6768	0.6829	-	0.6783	0.6836	-	0.6791	0.6848	-	0.6798	0.6853	-	0.6823	0.6855
ηr [-]	0.9992	0.9838	-	0.9997	0.9802	-	1	0.9795	-	1	0.9792	-	1	0.9789	-	1	0.9787	-
10KQ [-]	-	0.4217	0.4149	-	0.4163	0.4081	-	0.4145	0.406	-	0.4127	0.4041	-	0.4094	0.4008	-	0.4068	0.3981
KT [-]	-	0.2186	0.2165	-	0.2152	0.2129	-	0.2139	0.2112	-	0.2123	0.2096	-	0.2103	0.2076	-	0.2089	0.2054
tM [-]	0.1216	0.1203	-	0.1165	0.1152	-	0.1158	0.1146	-	0.1153	0.1155	-	0.1152	0.1176	-	0.1143	0.1208	-
wT [-]	0.1286	0.3152	-	0.1246	0.3203	-	0.1229	0.3208	-	0.1223	0.3214	-	0.1219	0.3216	-	0.1212	0.3212	-
ηh [-]	1.008	1.2846	-	1.0093	1.3018	-	1.0081	1.3036	-	1.008	1.3034	-	1.0076	1.3007	-	1.0079	1.2952	-
ηd [-]	0.6888	0.8483	-	0.6927	0.8636	-	0.6928	0.8661	-	0.6933	0.8667	-	0.6939	0.8656	-	0.6945	0.8649	-
ηi [-]	0.9476	-	-	0.9524	-	-	0.9541	-	-	0.9565	-	-	0.9573	-	-	0.9578	-	-
Pe [W]	267.651	267.651	-	1218.659	1218.659	-	1970.069	1970.069	-	3153.366	3153.366	-	4647.601	4647.601	-	6392.883	6392.883	-
Pd [W]	388.575	315.514	-	1759.289	1411.139	-	2843.633	2274.644	-	4548.342	3638.359	-	6697.796	5369.224	-	9205.015	7388.054	-

Table 6

Self-propulsion performance particulars for AFF-8 self-propulsion model.

	V_S = 2.75 m/s			V_S = 5.144 m/s			V_S = 6.096 m/s			V_S = 7.161 m/s			V_S = 8.231 m/s			V_S = 9.152 m/s		
Self-propulsion propeller modeling methods	Body force	Full geometric model	Comparison CFD OWCs	Body force	Full geometric model	Comparison CFD OWCs	Body force	Full geometric model	Comparison CFD OWCs	Body force	Full geometric model	Comparison CFD OWCs	Body force	Full geometric model	Comparison CFD OWCs	Body force	Full geometric model	Comparison CFD OWCs
J [-]	0.8663	0.7729	0.7729	0.8835	0.7823	0.7823	0.8886	0.7844	0.7844	0.8915	0.7881	0.7881	0.8943	0.7937	0.7937	0.8965	0.7972	0.7972
ηO [-]	-	0.6596	0.6631	-	0.6647	0.6685	-	0.6662	0.6694	-	0.6674	0.6712	-	0.6682	0.6724	-	0.6693	0.6735
ηr [-]	0.9956	0.9895	-	0.9975	0.9873	-	0.9972	0.9871	-	0.9968	0.987	-	0.9974	0.9869	-	0.9977	0.9869	-
10KQ [-]	-	0.4472	0.4425	-	0.4415	0.4359	-	0.4402	0.4345	-	0.4369	0.4312	-	0.4337	0.428	-	0.4305	0.4248
KT [-]	-	0.2397	0.2386	-	0.2357	0.2341	-	0.2349	0.2329	-	0.2325	0.2307	-	0.2294	0.2278	-	0.2271	0.2253
tM [-]	0.1285	0.1257	-	0.1239	0.1303	-	0.1236	0.1315		0.1224	0.1311	-	0.1228	0.1313	-	0.1217	0.1319	-
wT [-]	0.1262	0.3208	-	0.1243	0.3283	-	0.1233	0.3289	-	0.1238	0.3291	-	0.1241	0.3295	-	0.1245	0.3297	-
ηh [-]	0.9974	1.2873	-	1.0005	1.2948	-	0.9997	1.2941	-	1.0016	1.2951	-	1.0015	1.2956	-	1.0032	1.2952	-
ηd [-]	0.6791	0.8402	-	0.6834	0.8497	-	0.6828	0.851	-	0.6835	0.8531	-	0.6834	0.8544	-	0.6854	0.8469	-
ηi [-]	0.9269	-	-	0.9408	-	-	0.9412	-	-	0.9416	-	-	0.9423	-	-	0.9426	-	-
Pe [W]	247.264	247.264	-	1425.731	1425.731	-	2307.157	2307.157	-	3672.6	3672.6	-	5435.079	5435.079	-	7442.789	7442.789	-
Pd [W]	364.105	294.292	-	2086.232	1677.922	-	3378.965	2711.113	-	5373.226	4305.005	-	7951.835	6361.282	-	10859.04	8788.274	-

Heuristically, corresponding comparison CFD OWC results (Liwei Liu et al., 2021) have been included into Table 5 and 6 for calibrations and verifications in compliance with relevant self-propulsion vehicle velocities and propeller rotation speeds in six predetermined baseline self-propulsion points. With regard to both AFF-1 and AFF-8 cases, dimensionless amplified self-propulsion torque coefficient $10K_{QS}$, self-propulsion thrust coefficient K_{TS}, propeller advance coefficient J and open water propeller efficiency η_O estimated by means of full geometric model method are in line with corresponding comparison CFD OWC results well with fairly satisfying relative errors below 2.5% in general.

In addition, all propeller advance coefficient J and ideal propeller efficiency η_i presented in Table 5 are correspondingly higher than that in Table 6 while each amplified self-propulsion torque coefficient $10K_{QS}$, self-propulsion thrust coefficient K_{TS} and thrust deduction factor t_M arisen in Table 5 is correspondingly lower than that in Table 6, which seem to be attributed to AFF-8 appendage resistance influences quantified in Table 6.

Moreover, as for both AFF-1 and AFF-8 cases, amplified self-propulsion torque coefficient $10K_{QS}$, self-propulsion thrust coefficient K_{TS}, thrust deduction factor t_M, nominal wake coefficient w_T, hull efficiency η_h and propulsion efficiency η_d estimated by means of full geometric model method are correspondingly higher than that of body force method, which consistently certify that full geometric model method is more precise and promising for self-propulsion propeller detail modeling, flow velocity-pressure development characteristics description around self-propulsion models and self-propulsion simulation process rather than body force method.
In particular, relative rotation efficiency η_r and open water propeller efficiency η_O according to two self-propulsion propeller modeling methods shown in Table 6 are correspondingly lower than that in Table 5 on account of AFF-8 appendage resistance influences, which consequently brings about explicit lower hull efficiency η_h and propulsion efficiency η_d in Table 6 as expected. Furthermore, in general, propeller delivered power P_d according to two self-propulsion propeller modeling methods and effective power P_e presented in Table 6 are correspondingly higher than that in Table 5 due to AFF-8 appendage resistance influences and lower propulsion efficiency in AFF-8 cases while propeller delivered power P_d estimated by means of body force method in both AFF-1 and AFF-8 cases are correspondingly higher than that of full geometric model method for which is attributed to lower hull efficiency η_h and propulsion efficiency η_d from body force method.

5. Conclusions

In this paper, flow velocity-pressure development characteristics and pre-processing MTO CFD simulation on the foundation of two DARPA Suboff UV models (AFF-1 and AFF-8) and INSEAN E1619 propeller model are emphatically investigated.
With different tailored initial conditions, open water propeller analysis based upon MRF method, straight-ahead resistance simulation and self-propulsion simulation based upon thrust identity method have been respectively carried out using RANS Menter's k-ω SST mathematical turbulence model. In the sense of physics, turbulent boundary layer description for each CFD simulation case in this work has been optimized by means of Granville skin friction correction. As illustrated in chapter 4, in general, numerical results in regards to aforementioned three simulation cases show fairly satisfying agreement with corresponding available EFD validation data and most comparison CFD outcomes. In particular, AFF-8 appendage resistance influences are too significant and intricate to ignore in straight-ahead and self-propulsion cases while corresponding discretization error of CFD simulation solution, convergence rate and GCI uncertainty have been heuristically estimated, validated and studied on the basis of grid halving approach, discretization error methodology, FS approach and generalized RE method for both UV and propeller cases. In consideration of corresponding self-propulsion results, full geometric model method seems to be the preferred, applicable and promising option in self-propulsion interaction performance assessment at the expense of redundant computational overhead rather than body force method.
In future, more ITTC criteria, EFD validation data and comparison CFD outcomes will be obtained to sustain authenticity, reasonability, credibility and applicability of the work. Furthermore, in self-propulsion simulation, skew angle of E1619 propeller and training edge of AFF-8 stern fins will be flexibly tuned for further probable improvements with respect to relative rotation efficiency η_r and propulsion efficiency η_d.

6. Declarations

6.1 Ethics approval and consent to participate

We declare that researching methods in this paper strictly follows basic ethics principle, which can be responsible for supervising.

6.2 Consent for publication

We declare that the methods, materials and any other data in this paper are free to be published.

6.3 Availability of data and material

We declare that available investigating data, materials and methods appeared in this work can be allowed to be published and validated.

6.4 Competing interests

We declare that we have no financial and personal relationships with other people or organizations that can inappropriately influence our work. There is no professional or other personal interest of any product, service or company that could be construed as influencing the position presented in the review of the manuscript.

6.5 Authors' contributions

The author Fei Deng make available modeling, simulation and data analysis appeared in this paper based upon the instruction from Prof. Hongdong Yin. The paper is accomplished by Fei Deng, and revised by Fei Deng and Prof. Hongdong Yin.

Acknowledgements

The authors would like to express their gratitude to the Xiamen Institute of Software Technology and Earth Physics Laboratory of China University of petroleum (Beijing) for their financial support, and the editors and reviewers for their precious, rational and aided comments.

References

A. Drouet, G. Reliquet, A. Bardin, E. Jacquin, L. Gentaz, and B. Alessandrini, “Simulation of Submarine Manoeuvring Using NAVIER-STOKES Solver,” in *Proc. International Conference on Computational Methods in Marine Engineering*, Lisbon, Portugal, Sep. 2011.

Alejandro M. Castro, Pablo M. Carrica, and Frederick Stern, “Full scale self-propulsion computations using discretized propeller for the KRISO container ship KCS,” *J. Computers & Fluids*., vol. 51, pp. 35–47, Dec. 2011.

Alexander B Phillips, Stephen R Turnock, and Maaten Furlong, “Comparisons of CFD Simulations and In-service Data for the Self Propelled Performance of an Autonomous Underwater Vehicle,” in *Proc. 27th Symposium on Naval Hydrodynamics*, Seoul, Korea, Oct. 2008.

Alexander V. Inzartsev, *Underwater vehicles*. Slavka Krautzeka, Rijeka, Croatia: R. InTech, 2009.

A. Nakayama and V. C. Patel, *Calculation of The Viscous Resistance of Bodies of Revolution*. Iowa, USA: R. The University of Iowa, Oct. 1973.

B. Aupoix, “Wall Roughness Modelling with k-w STT Model,” in *Proc. 10th International ERCOFTAC Symposium on Engineering Turbulence Modelling and Measurements*, Marbella, Spain, Sep. 2014.

Bhushan Shanti, M. F. Alam, and D. K. Walters, “Evaluation of hybrid RANS/LES models for prediction of flow around surface combatant and Suboff geometries,” *J. Computers & Fluids*., vol. 88, pp. 834–849, Dec. 2013.

Chi Yang and Rainald Löhner, “Prediction of Flows over an Axisymmetric Body with Appendages,” in *Proc. 8th International Conference on Numerical Ship Hydrodynamics*, Busan, Korea, Sep. 2003.

Chunyu Guo, Xu Wang, Chongge Chen, Yinghong Li, and Jian Hu, “Numerical Investigation of Self-Propulsion Performance and Noise Level of DARPA Suboff Model,” *J. Journal of Marine Science and Engineering*., vol. 11, pp. 1–27, Jun. 2023.

Cihad Delen, Savas Sezen, and Sakir Bal, “Computational investigation of self propulsion performance of DARPA Suboff vehicle,” *J. Tamap Journal of Engineering*., pp. 1–12, Mar. 2017.

C. Liu, Y. Li, Z. Zhou, and P. Wiśniewski, “Effect of Cascade Surface Roughness on Boundary

Layer Flow Under Variable Conditions," *J. Frontiers in Energy Research*., vol. 9, pp. 1–13, Jan. 2022.
Cortana, *Description of Drag*. Falls Church, VA, USA: R. Cortana Corporation, Nov. 2013.
David C.Wilcox, *Turbulence modeling for CFD*. California, USA: M. DCW industries, 2006.
D. Dussin, M. Fossati, A. Guardone, and L. Vigevano, "Hybrid grid generation for two-dimensional high-Reynolds flows," *J. Computers & Fluids*., vol. 38, pp. 1863–1875, May. 2009.
Dmitriy Ponkratov and Constantinos Zegos, "Validation of ship scale CFD self-propulsion simulation by the direct comparison with sea trials results," in *Proc. Fourth International Symposium on Marine Propulsors SMP'15*, Austin, Texas, USA, Jun. 2015.
Dong Li, Qun Yang, Lin Zhai, Zhen Wang, and Chuan-lin He, "Numerical investigation on the wave interferences of submerged bodies operating near the free surface," *J. International Journal of Naval Architecture and Ocean Engineering*., vol. 13, pp. 65–74, Feb. 2021.
Ehsan Javanmard, Ehsan Yari, Javad A. Mehr, and Shahriar Mansoorzadeh, "Hydrodynamic characteristic curves and behavior of flow around a surface-piercing propeller using computational fluid dynamics based on FVM," *J. Ocean Engineering*., vol. 192, pp. 1–16, Nov. 2019.
Ehsan Yari and Hassan Ghassemi, "Hydrodynamic analysis of the surface-piercing propeller in unsteady open water condition using boundary element method," *J. International Journal of Naval Architecture and Ocean Engineering*., vol. 8, pp. 22–37, Jan. 2016.
Fabio Di Felice, Mario Felli, Mattias Liefvendahl, and Urban Svennberg, "Numerical and experimental analysis of the wake behavior of a generic submarine propeller," in *Proc. First International Symposium on Marine Propulsors SMP'09*, Trondheim, Norway, 2009.
Florian R. Menter, "Zonal two equation k-ω turbulence models for aerodynamic flows," in *Proc. 24th Fluid Dynamics Conference*, Orlando, Florida, USA, Jul. 1993.
Florian R. Menter, "Two-equation eddy-viscosity turbulence models for engineering applications," *J. Journal of American Institute of Aeronautics and Astronautics*., vol. 32, no. 8, pp. 1598–1605, Aug. 1994.
Frederick Stern, H. T. Kim, D. H. Zhang, Y. Toda, J. Kerwin, and S. Jessup, "Computation of viscous flow around propeller-body configurations: Series 60 C_B = 0.6 ship model," *J. Journal of Ship Research*., vol. 38, no. 2, pp. 137–157, Jun. 1994.
Frederick Stern, Robert Wilson, Hugh W. Coleman, and Eric Paterson, "Comprehensive Approach to Verification and Validation of CFD Simulations-Part 1: Methodology and Procedures," *J. Journal of Fluids Engineering*., vol. 123, no. 4, pp. 1–50, Dec. 2001.
Furkan KIYÇAK and Ömer Kemal KINACI, "Scale Effects On The Linear Hydrodynamic Coefficients of DARPA Suboff," *J. Journal of Naval Sciences and Engineering*., vol. 19, no. 1, pp. 53–76, Mar. 2023.
Gao Hongtao, Zhu Wencai, Liu Yutong, and YanYuying, "Effect of various winglets on the performance of marine propeller," *J. Applied Ocean Research*., vol. 86, pp. 246–256, May. 2019.
Grabert R, Lübke L, Klose R, and Barkmann U, *ITTC Propeller Benchmark PPTC Propeller VP1304*. Potsdam, German: R. Potsdam model basin, 2017.
Guanghua He, Cheng Zhang, Hongfei Xie, and Shuang Liu, "The Numerical Simulation of a Submarine Based on a Dynamic Mesh Method," *J. Journal of Marine Science and Engineering*., vol. 10, pp. 1–17, Oct. 2022.
Han-Lieh Liu and Thomas T. Huang, *Summary of DARPA Suboff Experimental Program Data*. West Bethesda, Maryland, USA: R. Carderock Division, Naval Surface Warfare Center, Jul. 1998.
Hermann Schlichting, *Boundary Layer Theory*. New York, USA: M. McGraw-Hill College, Apr. 1979.
Ismail B. Celik and Jun Li, "Assessment of Numerical Uncertainty for The Calculations of

995 Turbulent Flow Over A Backward Facing Step," in *Proc. Workshop on Uncertainty*
996 *Estimation*, Lisbon, Portugal, Oct. 2004.
997 Ismail B. Celik, U Ghia, Patrick J. Roache, and C. J. Freitas, "Procedure for Estimation and
998 Reporting of Uncertainty Due to Discretization in CFD Applications," *J. Journal of Fluids*
999 *Engineering*., vol. 130, no. 7, pp. 1–4, Jul. 2008.
1000 *ITTC, 1999, 00. 7.5-03-01-04, CFD verification*. S. ITTC Recommended Procedures and
1001 Guidelines, 1999.
1002 *ITTC, 2011, 02. 7.5-02-01-03, Fresh Water and Seawater Properties*. S. ITTC Recommended
1003 Procedures, 2011.
1004 "ITTC, 2011b, 01. 7.5-03-02-03, Practical guidelines for ship CFD applications," in *Proc.*
1005 *Presented at the Proceedings of 26th ITTC*, Hague, Netherlands, 2011.
1006 *ITTC, 2014, 00. 7.5-03-03-01, Practical Guidelines for Ship Self-Propulsion CFD*. S. ITTC
1007 Recommended Procedures and Guidelines, 2014.
1008 *ITTC, 2014, 03. 7.5-02-03-02.1, Open Water Test*. S. ITTC Recommended Procedures and
1009 Guidelines, 2014.
1010 *ITTC, 2017, 03. 7.5-03-01-01, Uncertainty analysis in CFD Verification and Validation*
1011 *Methodology and Procedures*. S. ITTC Recommended Procedures and Guidelines, 2017.
1012 J.C.Date and S.R.Turnock, *A Study into the Techniques Needed to Accurately Predict Skin Friction*
1013 *Using RANS Solvers with Validation against Froude's Historical Flat Plate Experimental*
1014 *Data*. Southampton, UK: R. University of Southampton, Mar. 1999.
1015 Jeong Hwa Seo, Dong Myung Seol, Ju Hyun Lee, and Shin Hyung Rhee, "Flexible CFD meshing
1016 strategy for prediction of ship resistance and propulsion performance," *J. International*
1017 *Journal of Naval Architecture and Ocean Engineering*., vol. 2, pp. 139–145, Sep. 2010.
1018 Jingyuan Li, Qinghe Zhang, and Tongqing Chen, "Numerical Investigation of Internal Solitary
1019 Wave Forces on Submarines in Continuously Stratified Fluids," *J. Journal of Marine Science*
1020 *& Engineering*., vol. 9, pp. 1–20, Dec. 2021.
1021 Ji Tao Qiu, Ning Li, Chen Jun Yang, You Lin Cai, and Kun Yu Meng, "Numerical study on a
1022 coupled viscous and potential flow design method of axial-flow pump impeller," *J. Ocean*
1023 *Engineering*., vol. 266, pp. 1–11, Dec. 2022.
1024 Jiyuan Tu, Guan Heng Teoh, and Chaoqun Liu, *Computational Fluid Dynamics A Practical*
1025 *Approach*. Waltham, USA: M. Butterworth-Heinemann, 2013.
1026 William L. Oberkampf and Christopher J. Roy, *Verification and Validation in Scientific Computing*.
1027 Cambridge, UK: M. Cambridge University Press, Oct. 2010.
1028 J.M.J. Journée and Jakob Pinkster, *Introduction in ship hydromechanics*. Delft, Netherlands: M.
1029 Delft University of Technology, 2002.
1030 J.M.J. Journée and W.W. Massie, *offshore hydromechanics*. Delft, Netherlands: M. Delft University
1031 of Technology, 2001.
1032 John C. Strikwerda, *Finite Difference Schemes and Partial Differential Equations (2nd)*. Madison,
1033 Wisconsin, USA: M. University of Wisconsin-Madison, 2004.
1034 Karim I, Rachmat G, Chuma N, and Naveed Khan N K, *Open Water Test of A Marine Propeller*.
1035 Trondheim, Norway: R. Norwegian University of Science and Technology, 2019.
1036 Kenshiro Takahashi, *Numerical Simulations of Comprehensive Hydrodynamic Performance of*
1037 *DARPA SUBOFF Submarine*. Melbourne, Florida, USA: D. Florida Institute of Technology,
1038 Dec. 2019.
1039 Leo Victor Lazauskas, *Hydrodynamics of Advanced High-Speed Sealift Vessels*. Adelaide,
1040 Australia: D. The University of Adelaide, Apr. 2005.
1041 LeVeque and Randall J, *Finite Difference Methods for Differential Equations*. Washington, USA:
1042 M. University of Washington, 2006.
1043 Liwei Liu, Meixia Chen, Jiawei Yu, Zhiguo Zhang, and Xianzhou Wang, "Full-scale simulation of
1044 self-propulsion for a free-running submarine," *J. Physics of Fluids*., vol. 33, pp. 1–15, Apr.

2021.
Luıs Eca and Martin Hoekstra, “Discretization Uncertainty Estimation based on a Least Squares version of the Grid Convergence Index,” in *Proc. 2nd Workshop on CFD Uncertainty Analysis*, Lisbon, Portugal, Oct. 2006.
Mattias Liefvendahl, “Investigation of Propeller Wake Instability using LES,” *J. Ship Technology Research*., vol. 57, pp. 100–106, Jan. 2015.
Mattias Liefvendahl, Niklas Alin, Michel Chapuis, Christer Fureby, Urban Svennberg, and Carl Troeng, “Ship and Propulsor Hydrodynamics,” in *Proc. V European Conference on Computational Fluid Dynamics ECCOMAS CFD*, Lisbon, Portugal, 2010.
Maxim Candries, *Drag, boundary-layer and roughness characteristics of marine surfaces coated with antifoulings*. Newcastle, UK: D. University of Newcastle-upon-Tyne, Dec. 2001.
Mojtaba Maali Amiri, *Numerical Evaluation of The Free Surface Effect On The Hydrodynamics and Dynamics of Underwater Vehicles*. Rio de Janeiro, Brasil: D. University Federal do Rio de Janeiro, 2018.
Nancy C. Groves, Thomas T. Huang, and Ming S. Chang, *Geometric characteristics of DARPA Suboff models*. West Bethesda, Maryland, USA: R. David W. Taylor Naval Ship Research and Development Center, Mar. 1989.
Nathan Chase, *Simulations of the DARPA Suboff submarine including self-propulsion with the E1619 propeller*. Iowa, USA: R. The University of Iowa, 2012.
Nathan Chase and Pablo M. Carrica, “Submarine propeller computations and application to self-propulsion of DARPA Suboff,” *J. Ocean engineering*., vol. 60, pp. 68–80, Mar. 2013.
Niklas Alin, Rickard E. Bensow, Christer Fureby, T. Huuva, and Urban Svennberg, “Current Capabilities of DES and LES for Submarines at Straight Course,” *J. Journal of Ship Research*., vol. 54, no. 3, pp. 184–196, Sep. 2010.
Pablo M. Carrica, Alejandro M. Castro, and Frederick Stern, “Self-propulsion computations using a speed controller and a discretized propeller with dynamic overset grids,” *J. Journal of Marine Science and Technology*., vol. 15, pp. 316–330, Aug. 2010.
Patrick J. Roache, “Quantification of Uncertainty in Computational Fluid Dynamics,” *J. Annual Review of Fluid Mechanics*., vol. 29, pp. 123–160, Jan. 1997.
Patrick J. Roache, “Verification of Codes and Calculations,” *J. Journal of American Institute of Aeronautics and Astronautics*., vol. 36, no. 5, pp. 696–702, May. 1998.
Paul S. Granville, *Drag and Turbulent Boundary Layer of Flat Plates at Low REYNOLDS NUMBERS*. West Bethesda, Maryland, USA: R. David W. Taylor Naval Ship Research and Development Center, 1989.
Philippe G. Ciarlet, *The Finite Element Method for Elliptic Problems*. Amsterdam, Netherlands: M. North Holland, 1978.
Pijush K. Kundu and Ira M. Cohen, *fluid mechanics*. Burlington, MA, USA: M. Elsevier, 2008.
Robert F. Roddy, *Investigation of The Stability and Control Characteristics of Several Configurations of The DARPA Suboff Model (DTRC Model 5470) From Captive-Model Experiments*. West Bethesda, Maryland, USA: R. David W. Taylor Naval Ship Research and Development Center, Sep. 1990.
Serge Toxopeus, “Viscous-flow calculations for bare hull DARPA SUBOFF submarine at incidence,” *J. International Shipbuilding Progress*., vol. 55, no. 3, pp. 227–251, 2008.
Sinan Burunsuz, M. Cansin Ozden, Yasemin Arikan Ozden, and Ismail Hakki Helvacioglu, “Four Quadrant Thrust and Torque Prediction of INSEAN E-1619 Generic Submarine Propeller for Submarine Maneuvering Simulations,” in *Proc. Fifth International Symposium on Marine Propulsors SMP’17*, Espoo, Finland, Jun. 2017.
Tahsin Tezdogan, Yigit Kemal Demirel, Paula Kellett, Mahdi Khorasanchi, Atilla Incecik, and Osman Turan, “Full-scale unsteady RANS CFD simulations of ship behaviour and performance in head seas due to slow steaming,” *J. Ocean Engineering*., vol. 97, pp. 186–206,

Jan. 2015.
Tao Xing and Frederick Stern, *Factors of Safety for RICHARDSON EXTRAPOLATION*. Iowa, USA: R. The University of Iowa, Mar. 2009.
Theodore von Kármán, "Turbulence and Skin Friction," *J. Journal of the Aeronautical Sciences*., vol. 1, no. 1, pp. 1–20, Jan. 1934.
Thomas T. Huang, Han-Lieh Liu, and Nancy C. Groves, *Experiments of The DARPA Suboff Program*. West Bethesda, Maryland, USA: R. David W. Taylor Naval Ship Research and Development Center, Dec. 1989.
Tran Ngoc Tu, "Numerical simulation of propeller open water characteristics using RANSE method," *J. Alexandria Engineering Journal*., vol. 58, pp. 531–537, Jun. 2019.
Tyrone S. Phillips and Christopher J. Roy, "Richardson Extrapolation-based Discretization Uncertainty Estimation for Computational Fluid Dynamics," *J. Journal of Fluids Engineering*., vol. 136, no. 12, pp. 1–17, Sep. 2014.
Vladimir I. Krasilnikov, "Self-Propulsion RANS Computations with a Single-Screw Container Ship," in *Proc. Third International Symposium on Marine Propulsors SMP'13*, Launceston, Tasmania, Australia, May. 2013.
Volker Bertram, *Practical Ship Hydrodynamics*. Woburn, UK: M. Butterworth-Heinemann, 2000.
Xuting Zhang, Yi Hong, Fan Yang, Weicheng Jiao, and Rongguo Wang, "Effect of rudder on propulsion performance and structural deformation of composite propellers," *J. Ocean Engineering*., vol. 182, pp. 318–328, Jun. 2019.
Xuting Zhang, Yi Hong, Fan Yang, Weicheng Jiao, and Rongguo Wang, "Effect of rudder on propulsion performance and structural deformation of composite propellers," *J. Ocean Engineering*., vol. 182, pp. 318–328, Jun. 2019.
Yan Naing Win, Emel Tokgoz, Ping-Chen Wu, Frederick Stern, and Yasuyuki Toda, "Computation of propeller-hull interaction using simple body-force distribution model around Series 60 C_B = 0.6," *J. Journal of the Japan Society of Naval Architects and Ocean Engineers*., vol. 18, pp. 17–27, Jan. 2013.
Yasemin Arıkan Ozden, Munir Cansın Ozden, Ersin Demir, and Sertaç Kurdoglu, "Experimental and Numerical Investigation of DARPA Suboff Submarine Propelled with INSEAN E1619 Propeller for Self-Propulsion," *J. Journal of Ship Research*., vol. 63, no. 4, pp. 235–250, Dec. 2019.
Yasemin Arıkan Ozden, Munir Cansın Ozden, and Fahri Çelik, "Numerical Investigation of Submarine Tail Form on the Hull Efficiency," in *Proc. Fifth International Symposium on Marine Propulsors SMP'17*, Espoo, Finland, Jun. 2017.
Yigit Kemal Demirel, Mahdi Khorasanchi, Osman Turan, Atilla Incecik, and Michael P. Schultz, "A CFD model for the frictional resistance prediction of antifouling coatings," *J. Ocean Engineering*., vol. 89, pp. 21–31, Jul. 2014.
Yu-Hsin Lin and Ahmad Darori Hasan, "The CFD simulation of E1619 propeller open-water tests validated by the EFD in the NCKU towing tank," *J. Journal of Mechanics*., vol. 39, pp. 416–430, Nov. 2023.
Yung An Chu, Chun Ta Lin, Ching Yeh Hsin, and Ya Jung Lee, "Numerical Analysis of Propulsion for Submarine with Highly Skewed Propeller," in *Proc. Proceedings of 8th PAAMES and AMEC*, Busan, Korea, 2018.
Yusuke Tahara, Robert V. Wilson, Pablo M. Carrica, and Frederick Stern, "RANS simulation of a container ship using a single-phase level-set method with overset grids and the prognosis for extension to a self-propulsion simulator," *J. Journal of Marine Science and Technology*., vol. 11, pp. 209–228, Dec. 2006.

Supplementary Files

This is a list of supplementary files associated with this preprint. Click to download.

- Highlights.docx
- Experimentaldatafiles.rar
- Nomenclaturesandnotations.rar
- Openwaterpropelleranalysisfile.rar
- PreprocessingMTOconvergenceanduncertaintyfiles.rar
- Straightaheadresistancesimulationfiles.rar
- Selfpropulsionsimulationfiles.rar